Chirped fields for Rb+Cs photoassociation

A. Homer and G. Roberts
Department of Physics, University of Newcastle, Newcastle upon Tyne NE1 7RU, United Kingdom
(Received 4 July 2008; published 11 November 2008)

This paper presents model numerical simulations of photoassociation and ionization of cold Rb+Cs atoms steered by broadband optical pulses operating within the weak-field limit over a picosecond time scale. The primary focus of the work is on generation of RbCs molecules in bound levels of the $(1)0^+$ $(X^1\Sigma^+)$ electronic ground state through a sequence of pump-dump transitions between $(1)0^+$ and $(4)0^+$ states driven by a field centered at 811 nm with different phase modulations. It is found that chirped fields generate substantially bound oscillator levels of the $X^1\Sigma^+$ state by avoiding promotion of amplitude to vibrational levels in the upper state whose Franck-Condon factors for stimulated emission to levels in the $X^1\Sigma^+$ state are detrimentally low, but which otherwise come into play when the driving field is transform limited. Optimal generation of molecules in the electronic ground state irrespective of vibrational level selectivity is calculated to occur when the temporal phase of the driving field is modulated by the classical energy difference for promotion of $(4)0^+ \leftarrow (1)0^+$ photon absorption. Conversely, generation of deeply bound vibrational eigenlevels of the $X^1\Sigma^+$ state is optimally promoted by a field whose temporal phase enhances $(4)0^+ \rightarrow (1)0^+$ stimulated emission. Driving fields phase modulated by the classical difference potential or linearly down-chirped enhance molecule formation vis-à-vis the thermal collision; fields whose temporal phase is modulated according to the shape of the $(1)0^+$ potential energy curve or which are linearly up-chirped suppress molecule formation relative to the thermal probability, but generate deeply bound $X^1\Sigma^+$ vibrational levels. Application of a bichromatic field comprising temporally overlapped components centered 811 and 622 nm also improves the probability of generating deeply bound vibrational levels, but at the expense of increased ionization. Model calculations of transition probabilities between neutral and ionic states of the collision lead to the conclusions that: transitions to individual vibrational levels of the $X^1\Sigma^+$ state occur with a higher probability than resonant three-photon ionization prompted by a single-color field at 811 nm; and application of bichromatic light at 811 and 622 nm preferentially ionizes the incipient molecule via a two-color two-photon absorption, the likelihood of which masks the occupation of deeply bound $X^1\Sigma^+$ oscillator levels.

DOI: 10.1103/PhysRevA.78.053404 PACS number(s): 32.80.Qk

I. INTRODUCTION

Recent years have witnessed a proliferation in the number and types of problems in atomic physics to which coherent control strategies involving tailored light pulses have been applied [1]. Problems demanding control over both external and internal atomic degrees of freedom have been tackled by experiment and theoretical calculation. One particular interest has been the application of shaped **E** fields to assist formation of molecules in specified quantum states by preferentially steering photoassociation in cold atomic gases and Bose-Einstein condensates (BECs) [2], the motivation for which resides in the potential of cold molecules to serve as a vehicle for investigations of a range of fundamental problems. These include high-precision spectroscopy for measurements of the constants of nature [3], violations of parity and time (PT) inversion [4], and tests of quantum nonlocality through measurements of pair-wise atomic correlation functions [5]. Cold molecular matter also offers opportunities for quantum information processing [6] and investigations of quantum many-body correlations [7].

Considerable theoretical effort has been devoted to investigating the effect of frequency-swept field collisions in cold and ultracold atomic gases. In the earliest general scheme to receive attention, an atomic pair is promoted by a phase-modulated field to an excited electronic state from which a fraction of spontaneous emission results in bound molecules in highly excited oscillator levels supported by the electronic ground state [8,9]. In an attempt to avoid, or at least alleviate, the lack of vibrational state specificity inherent to spontaneous emission between molecular electronic states, later proposals have taken advantage of stimulated absorption and emission to steer atoms into more deeply bound levels which are not so prone to redissociation and other external perturbations [9,10]. Theory has also explored the effect of sequences of shaped optical fields to drive population into deeply bound levels by stimulated adiabatic passage or coherent accumulation, where near unity transfer efficiencies have been calculated [11]. The adiabatic passage approach has been applied successfully in the laboratory by Danzl *et al.*, who generated $n=73$ Cs_2 in the $X^1\Sigma_g^+$ electronic ground state starting from a Feshbach resonance in a BEC [12].

Experimental studies of coherent control of cold atomic collisions have been carried out with narrowband and broadband light sources. The application of linear frequency sweeps across atomic resonance transitions has been demonstrated to affect the rate of inelastic collisional loss of atoms from a magneto-optical trap (MOT) [13]. As noted elsewhere [10(d),13(c)], the implementation of broadband photoassociation by tailoring the **E** field of femtosecond light to the local Hamiltonian has so far hindered the generation of molecules compared to the rate of formation at thermal equilibrium; and a similarly discouraging prospect is found on comparison with the rates stimulated by transform-limited pulses

and continuous-wave (cw) fields [14]. Broadband fields have nevertheless been employed under algorithmic control to change the photoexcitation and ionization properties of ultracold molecules [14(b), 14(c)] and to investigate the time dependence of the coherent light-molecule interaction [14(d)]. Viteau *et al.* have applied shaped broadband fields to cool Cs_2 molecules generated beforehand by cw photoassociation and spontaneous emission, thereby transferring 70% of the molecular population into the zero-point level of the $X^1\Sigma_g^+$ state [14(e)].

Experimental and theoretical investigations of photoassociation [8–10,14] driven by broadband light fields have focused on formation of molecules in an isotopically pure atomic gas, predominantly those of Rb and Cs, partly because of the convenient overlap of resonant atomic transitions with current laser sources and the difficulty of loading different atoms into a MOT, and partly because of the availability of spectroscopically tested potential curves for different electronic interactions [15]. The light-assisted collision of interest in this work is that between ^{85}Rb and ^{133}Cs atoms driven by a broadband laser field centered at $\lambda_0 = 811 \pm 27$ nm [16]. The calculations presented here seek to provide a model theoretical assessment of photoassociation through the provision of a set of realistic simulations to determine pulse shapes (un)suited for photoassociation, especially those adapted to generate deeply bound vibrational levels of the $X^1\Sigma^+$ molecular state. With this goal in mind, the effect of a bichromatic field comprising components at 811 and 622 nm is compared to application of the near-infrared field alone.

Photoassociation of Rb+Cs resulting in generation of the zero-point level of the $X^1\Sigma^+$ electronic ground state, as well as the lowest triplet $a^3\Sigma^+$ state, has been achieved in the laboratory by a scheme which requires three separate cw laser beams [17]. In contrast to these studies, in which photoassociation was initiated by excitation of the $6p_{1/2,3/2} \leftarrow 6s_{1/2}$ Cs transitions, the photoassociation scheme considered here is constructed about the $5p_{1/2} \leftarrow 5s_{1/2}$ Rb transition at 795.0 nm encompassed by the bandwidth of the driving field. Figure 1(a) shows potential curves relevant to this study. Correlating with the $5p_{1/2}$ Rb+$6s_{1/2}$ Cs atomic levels are the $(4)0^+$, $(4)0^-$, and (5)1 electronic states of Rb+Cs [18], here labeled according to Hund's case (c) coupling scheme, which lead diabatically to the $3^1\Sigma^+$ and $3^3\Sigma^+$ bound-atom states in Hund's case (a) notation [19]. To assess the facility of photoassociation driven by broadband laser pulses, the $(4)0^+$ potential was adopted as a representative excited-state atomic interaction so as to avoid spin-forbidden $3^3\Sigma^+ \leftrightarrow X^1\Sigma^+$ transitions at atomic separations where Hund's case (a) coupling is prevalent; the difference in well depths and anharmonicities between the $3^1\Sigma^+$ and $3^3\Sigma^+$ bound states is shown in the inset to Fig. 1(a). From herein we adopt the notation for electronic states explained in Ref. [22]. Franck-Condon factors for transitions from vibrational levels of the $3^1\Sigma^+$ state of interest in this work to all levels of the $X^1\Sigma^+$ state are displayed in Fig. 1(b).

Care was taken in these calculations to impose strict weak-field conditions so that the effects of different chirps could be understood in terms of simple results from perturbation theory: the paper is intended to provide an initial framework from which more sophisticated control schemes for photoassociation of Rb+Cs by broadband fields may be formulated in the future. Although the principal focus of this work is concerned with mapping out routes for production of RbCs molecules in deeply bound vibrational levels of the ground electronic state, we also examine the relative efficiencies of ionization vis-à-vis association so as to assess their relative likelihood given the starting conditions selected here: the motivation for the comparison is that photoionization is often adopted [23] as a diagnostic probe for detection of molecular configurations in cold gases. The balance of the paper is organized as follows: Sec. II describes the general theoretical aspects of the wave-packet calculations, details of which are supplied in the Appendix; the relative populations in different electronic and vibrational levels generated by different light fields are presented and discussed in Sec. III; a summary of the findings concerning Rb+Cs photoassociation by chirped fields to emerge from the calculations is provided in Sec. IV.

II. THEORETICAL APPROACH

A. Probability amplitudes

Probability amplitudes for photon absorption and emission between the neutral states $|0\rangle$ and $|1\rangle$ and the ion state $|2\rangle$ were calculated up to third order in the perturbation due to the field. The amplitude $A^{(1)}_{1\leftarrow 0}(t)$ for $|1\rangle \leftarrow |0\rangle$ single-photon absorption was computed from

$$A^{(1)}_{1\leftarrow 0}(t) = -i \exp[i\phi_{1,0}(t,t_0)] \int_{t_0\rightarrow -\infty}^{t} \langle 1(t_1)|\tilde{V}(t_1)|0(t_1)\rangle dt_1, \tag{1}$$

where $\tilde{V}(t_1) = \tilde{V}_0^*(t_1)\exp[-i\omega_0 t_1]$ is the perturbation for photon absorption at time t_1, $\phi_{1,0}(t,t_0)$ is a phase which depends on the initial and final states at times t and t_0, and we set $\hbar = 1$ throughout. The amplitude of a pump-dump sequence of photon-atom interactions to generate molecules in their ground electronic state was calculated from the second-order expression

$$\begin{aligned} A^{(2)}_{0\leftarrow 0}(t) = &-\exp[-i\omega_0(t-t_0)] \\ &\times \int_{t_0\rightarrow -\infty}^{t} \int_{t_0\rightarrow -\infty}^{t_1} \langle 0(t_1)|\tilde{V}(t_1) U_1^{(0)}(t_1,t_2) \\ &\times \tilde{V}(t_2)|0(t_2)\rangle dt_1 dt_2, \end{aligned} \tag{2}$$

with $\tilde{V}(t_2) = \tilde{V}_0^*(t_2)\exp[-i\omega_0 t_2]$ and $\tilde{V}(t_1) = \tilde{V}_0(t_1)\exp[i\omega_0 t_1]$. The time-evolution operator $U_1^{(0)}(t_1,t_2) = |1(t_1)\rangle\langle 1(t_2)| = \exp[-iH_1(t_1-t_2)]$ propagates the molecule over the excited-state potential $V_1(R)$ between perturbations. Calculation of $A^{(2)}_{0\leftarrow 0}(t)$ permits distinction between pump-dumped amplitude in the ground electronic state and amplitude "already there" (i.e., the zeroth-order state) due to the slow thermal approach of the atoms over the $(1)0^+$ potential curve. The amplitudes of two- and three-photon ionization are

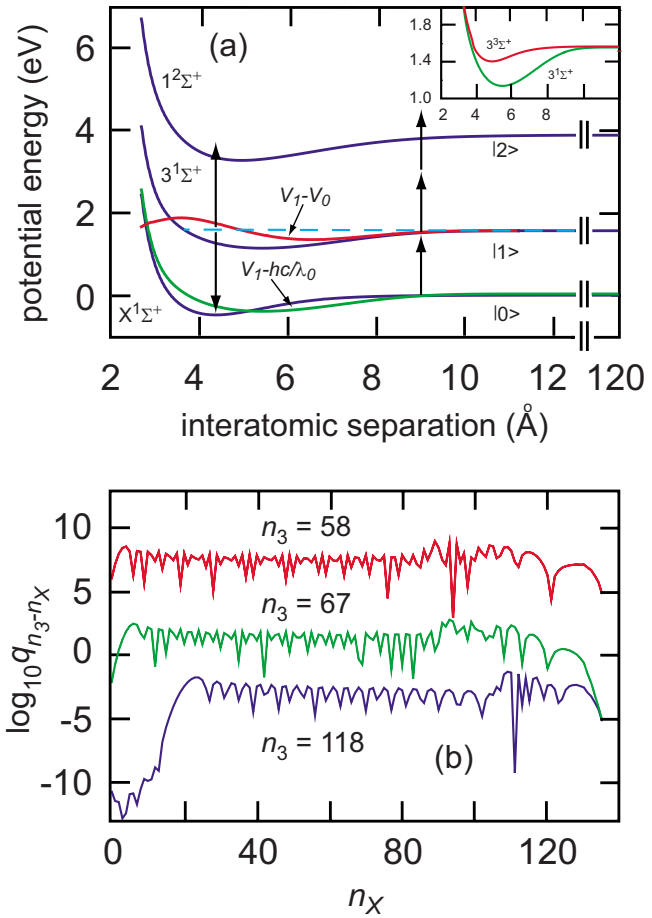

FIG. 1. (Color online) (a) Potential energy curves for Rb+Cs and Rb+Cs$^+$ collisions in electronic states relevant to photoassociation by a broadband laser pulse centered at $\lambda_0=811\pm27$ nm. Potential curves for the $(1)0^+$ and $(4)0^+$ electronic states which correlate with the $X^1\Sigma^+$ and $3^1\Sigma^+$ bound states of the neutral molecule are displayed in the main body of the diagram and are designated $|0\rangle$ and $|1\rangle$, respectively; the $(1)0^+$ ground state of the ion is $|2\rangle$. The inset at top right displays the potential curves which correlate asymptotically with separate $5p_{1/2}$ Rb+$6s_{1/2}$ Cs atoms: the $(4)0^+\leftrightarrow 3^1\Sigma^+$ curve is shown in green, the degenerate $(4)0^-$, $(5)1\leftrightarrow 3^1\Sigma^+$ curve in red. Potential curves were constructed from relativistic *ab initio* data points provided at the website http://lasim.univ-lyon1.fr/allouche/rbcs-so.htm discussed in Ref. [18]. The difference potential and detuning $V_1(R)-hc/\lambda_0$ are displayed by the red and green curves, respectively, in the main body of the diagram. The horizontal (light blue) dashed line indicates the energy deposited in the Rb+Cs collision by photon absorption at $R=9.1$ Å (see text). The vertical arrows indicate the energetics of three-photon ionization of $|0\rangle$ at 811 nm on the right and single-photon ionization and stimulated emission from $|1\rangle$ at 622 nm on the left. (b) Franck-Condon factors $q_{n_3-n_X}$ calculated from the program of Ref. [21] for transitions from vibrational levels $n_3=118$ (blue curve), 67 (green curve), and 58 (red curve) of the $3^1\Sigma^+$ state to all vibrational levels n_X of the $X^1\Sigma^+$ state. The selected levels of the $3^1\Sigma^+$ state are those maximally populated by 1 ps driving fields centered at $\lambda_0=811$ nm with temporal phase modulations $d\phi(t)/dt=0$ $(n_3=118)$, $d\phi(t)/dt=\Delta V_1[\langle R_1\rangle(t)]-\omega_0$ $(n_3=67)$ and $\Delta V_1[\langle R_0\rangle(t)]-\omega_0$ $(n_3=58)$. The curve for $n_3=58$ is displaced by $\log_{10} q_{58-n_X}+10$ and the curve for $n_3=67$ by $\log_{10} q_{67-n_X}+4$ for clarity.

$$A^{(2)}_{2\leftarrow0}(\varepsilon_{\mathbf{k}};t)=-\exp[i\phi_{2,0}(t,t_0)]\int_{t_0\rightarrow-\infty}^{t}\int_{t_0\rightarrow-\infty}^{t_1}\langle 2(t_1;\varepsilon_{\mathbf{k}})|\times\tilde{V}(t_1;\varepsilon_{\mathbf{k}})U^{(0)}(t_1,t_2)\tilde{V}(t_2)|0(t_2)\rangle dt_1dt_2, \quad (3a)$$

$$A^{(3)}_{2\leftarrow0}(\varepsilon_{\mathbf{k}};t)=i\exp[i\phi_{2,0}(t,t_0)]\times\int_{t_0\rightarrow-\infty}^{t}\int_{t_0\rightarrow-\infty++}^{t_1}\int_{t_0\rightarrow-\infty}^{t_2}\langle 2(t_1;\varepsilon_{\mathbf{k}})|\times\tilde{V}(t_1;\varepsilon_{\mathbf{k}})U^{(0)}(t_1,t_2)\tilde{V}(t_2)U^{(0)}(t_2,t_3)\times\tilde{V}(t_3)|0(t_3)\rangle dt_1dt_2dt_3, \quad (3b)$$

where $\tilde{V}(t)=\tilde{V}_0^*(t)\exp[-i\omega_0 t]$ for all perturbations and the $U^{(0)}(t_i,t_j)$ propagate wave functions via real or virtual states as appropriate. Equations (1)–(3) employ the formal time sequence $t_1>t_2>t_3$ and $\tilde{V}_0(t)=-\mathbf{d}\cdot\tilde{\boldsymbol{\mathcal{E}}}(t)$ is the complex interaction amplitude within the dipole approximation. The probability amplitudes $A^{(r)}_{q\leftarrow0}(t)$ calculated to rth order link the nuclear vector states $|\Psi^{(r)}_q(t)\rangle$ associated with the $|q\rangle$ within the Born-Oppenheimer approximation to the starting state $|\Psi^{(0)}_0(t_0)\rangle$ by

$$|\Psi^{(r)}_q(t)\rangle=A^{(r)}_{q\leftarrow0}(t)|\Psi^{(0)}_0(t_0)\rangle;$$

the corresponding nuclear wave functions are $\psi^{(r)}_q(R;t)=\langle R|\Psi^{(r)}_q(t)\rangle$.

Calculated from the transition amplitudes of Eqs. (1) and (2) were the probabilities $P^{(r)}_{q\leftarrow0}(t)=|A^{(r)}_{q\leftarrow0}(t)|^2$ of transitions connecting the starting state to $|1\rangle$ and back to $|0\rangle$ and $p_n(t)=|\langle n|\Psi^{(r)}_q(t)\rangle|^2$ for promoting population in bound vibrational levels $|n\rangle$ supported by the potentials of $|q\rangle$. Equations (3) enable calculation of the energy-resolved ionization probability

$$P^{(r)}_{2\leftarrow0}(\varepsilon_{\mathbf{k}};t)=|A^{(r)}_{2\leftarrow0}(\varepsilon_{\mathbf{k}};t)|^2, \quad (4)$$

where we have set $\|\Psi^{(0)}_0(t_0)\|^2=1$, and the energy-integrated ionization probability

$$P^{(r)}_{2\leftarrow0}(t)=\int_0^{\varepsilon_{\mathbf{k}_{\max}}}P^{(r)}_{2\leftarrow0}(\varepsilon_{\mathbf{k}};t)d\varepsilon_{\mathbf{k}}. \quad (5)$$

At each $\varepsilon_{\mathbf{k}}$, $P^{(r)}_{2\leftarrow0}(\varepsilon_{\mathbf{k}};t)$ includes the contributions of nonresonant $|2\rangle\leftarrow|0\rangle$ ionization, resonant ionization via $|1\rangle$, and their mutual interference. The integral over kinetic energy in Eq. (5) was approximated by summing values of $P^{(r)}_{2\leftarrow0}(\varepsilon_{\mathbf{k}})$ calculated at discretized values of $\varepsilon_{\mathbf{k}}$ differing at most by 160 meV, this being the energy separation used to calculate the Hamiltonian of the ion. Information on the Hamiltonian operators and transition dipole moments used to construct the operators $\tilde{V}(t)$ and $U^{(0)}(t_i,t_j)$ which appear in the integrands of Eqs. (1)–(3) is provided in Secs. I and II of the Appendix.

B. Photoassociating field parameters

In all calculations we take the photoassociating field $\mathbf{E}(t)=-\partial\mathbf{A}(t)/\partial t$ to be linearly polarized along the direction

of $\mathbf{d}_{1\leftarrow 0}$ and $\mathbf{d}_{2\leftarrow 0}$ with a vector potential $\mathbf{A}(t)=-(1/\omega_0)\mathrm{Im}\{\tilde{\boldsymbol{\mathcal{E}}}(t)\exp[i\omega_0 t]\}$ and $\tilde{\boldsymbol{\mathcal{E}}}(t)=\mathbf{E}_0\exp[-t^2/\sigma^2+i\phi(t)]$. The main perceived advantage of using femtosecond lasers for light control of cold-atom collisions is perhaps that the temporal phase $\phi(t)$ of a train of pulses can be actively manipulated to generate fields tailored to the Hamiltonians of the colliding atoms in different optically accessible states [1,8–10,14]. To investigate the possibilities for steering Rb+Cs collisions into bound quantum states, three types of temporal phase variation are considered in this work.

1. Potential-matched phases

A temporal phase modulated by the energy difference between optically connected states facilitates a Raman walk [10(c)] of amplitude into the ground electronic state at $R \leqslant 10$ Å through successive pump-dump scatterings during the pulse width. Two energy differences are studied in this investigation: the first matches $\phi(t)$ to the classical difference potential $\Delta V_1[R(t)]=V_1[R(t)]-V_0[R(t)]$ according to

$$\phi(t)=\int_{-\infty}^{t}\{\Delta V_1[R(t')]-\omega_0\}dt'; \tag{6}$$

the second references $\phi(t)$ to the variation of the ground-state potential $V_0[R(t)]$ with respect to the potential energy $V_1(R_0)$ of the excited state at the starting coordinate R_0 via

$$\phi(t)=\int_{-\infty}^{t}\{\Delta V_2[R(t')]-\omega_0\}dt', \tag{7}$$

where $\Delta V_2[R(t)]$ designates $V_1(R_0)-V_0[R(t)]$. The modulation of $\phi(t)$ by Eq. (7) aims to provide an instantaneous frequency which optimizes stimulated emission to bound levels of the $X^1\Sigma^+$ state as the wave packet in the $(4)0^+$ state tracks across $V_1(R)$.

Judging from the graph of $\Delta V_1(R)$ as a function of R presented in Fig. 1(a), the intuitive expectation would be that $\phi(t)$ given by Eq. (6) be first red chirped and then blue chirped as wave packets in the $X^1\Sigma^+$ and $3^1\Sigma^+$ electronic states depart from R_0 towards their inner turning points. The variation of $V_0(R)$ with R contrarily suggests that when $\phi(t)$ is given by Eq. (7), the time-dependent frequency of the driving field be blueshifted at all times during the evolution of $\psi_1^{(1)}(R;t)$ from R_0 to its inner turning point where the spread of amplitude is centered at 5.1 Å. In all calculations where the phase modulation applied to $\tilde{\boldsymbol{\mathcal{E}}}(t)$ followed Eqs. (6) or (7), the temporal width of the pulse was chosen to be $\sigma=1$ ps to allow enough time for the nuclear wave packet in the excited neutral state to complete at least one oscillation above the potential well of the ground state. In this way, application of a chirped field whose pulse width is similar to the wave-packet oscillation period serves to enhance the transfer of amplitude during a time period of restricted duration. The lower limit appended to the integrals of Eqs. (6) and (7) formally represents a time infinitely long ago in the causal past where the field nominally had a phase to which $\phi(t)$ at subsequent times is referred. To evaluate the integrals in Eqs. (6) and (7), the location $R(t)$ was replaced by the expectation value $\langle R_q\rangle(t)=\langle\psi_q(t)|R|\psi_q(t)\rangle$ of the interatomic separation in the qth electronic state: the accuracy of this replacement is discussed in Sec. III of the Appendix.

2. Quadratic phases

Whereas generation of a potential-matched phase of the form discussed above requires, in the laboratory, active manipulation of $\phi(t)$ by adaptive optics at different times during $\mathbf{E}(t)$ to optimize the collisional evolution, a quadratic phase can be imposed on $\tilde{\boldsymbol{\mathcal{E}}}(t)$ in a more straightforward manner by a linear dispersion line equipped with a grating pair. Figure 1(a) indicates that when the wave packet $\psi_0^{(0)}(R;t)$ begins its inwards-bound trajectory, the potential difference it experiences decreases from $V_1-V_0=1.530$ eV at $R=9.1$ Å to a minimum gap of $V_1-V_0=1.346$ eV at $R=6.6$ Å. A wave-packet subject to the attractive force of the $X^1\Sigma^+$ state at $R<9.1$ Å reaches $R\simeq 6.6$ Å after about 1.25 ps at $T=2$ mK. Linearizing the classical potential difference between $|1\rangle$ and $|0\rangle$ over this time would suggest optimal application of a field with a quadratic phase $\phi(t)=-\beta t^2/\sigma^2=-1.1092\times 10^{-4}t^2$ [fs]^2 rad. An alternative proposal recognizes that the wave packet $\psi_1^{(1)}(R;t)$ in the excited state reaches $R=4.4$ Å, where its center is located above the ground-state minimum, after about 1.5 ps, at which point the energy difference $\langle\psi_1^{(1)}(R_0;t)|V_1|\psi_1^{(1)}(R_0;t)\rangle-V_0(R)$ is 1.993 eV. In this case, linearizing the attractive limb of $V_0(R)$ would suggest application of a phase modulation $\phi(t)=2.3514\times 10^{-4}t^2$ [fs]^2 rad to the driving field to promote ground-state molecule formation.

To investigate the effect of linearly up- and down-chirped pulse on Rb+Cs population dynamics, the above values of β/σ^2 were maintained in fields with $\sigma=175$, 355, and 530 fs for down chirps and $\sigma=83$, 167, and 250 fs for up chirps, thereby giving time-dependent frequencies $\omega(t)=\omega_0\pm n\Delta\omega$ $(n=1-3)$, which differed from the carrier by an integer number of Fourier bandwidths $\Delta\omega$ between the beginning $(t=-2\sigma)$ and temporal midpoint $(t=0)$ of each pulse; in this way, $\omega(t)$ attained its minimum or maximum frequency when the pulse intensity was maximal.

3. A constant phase

The photoassociative capability of unchirped fields with pulse widths $\sigma=1$ ps and 30 fs [16] was investigated to provide a baseline against which enhancements in population transfer between $|1\rangle$ and $|0\rangle$ driven by fields with the temporal phases described in Sec. II B 1 and Sec. II B 2 above could be assessed.

To ensure that the interaction between light and colliding atoms was maintained under weak-field conditions, a maximum field strength $|\mathbf{E}_0|$ was selected so that $|\langle 1|\mathbf{d}\cdot\tilde{\boldsymbol{\mathcal{E}}}(t)|0\rangle|$ and $|\langle 2|\mathbf{d}\cdot\tilde{\boldsymbol{\mathcal{E}}}(t)|0\rangle|$ remained smaller than the expectation values $\langle q|H_q|q\rangle$ and $\langle q;\varepsilon_{\mathbf{k}}|H_q|q;\varepsilon_{\mathbf{k}}\rangle$ at all times during the pulse evolution. From such a comparison, it was found that the $|1\rangle\leftrightarrow|0\rangle$ transition necessitated application of the smallest fields strengths to operate under weak-field conditions. Accordingly, a value of $|\mathbf{E}_0|=2.5\times 10^{-4}$ a.u. $(\cong 1.29\times 10^8$ V/m, maximum intensity $I_0\simeq 2.2$ GW/cm$^2)$ was adopted such that $|\langle 1|\tilde{V}(t)|0\rangle|$ was at most two times smaller

than the smallest value of $|\langle 0|-\nabla^2/2+V_0|0\rangle|$ for motion of Rb+Cs over the ground electronic potential.

In all calculations with a single-color photoassociation field, the bandwidth at 811 nm was taken to be $\Delta\lambda=27$ nm, commensurate with a Fourier-limited full width at half maximum (FWHM) of 35.322 fs ($\sigma=30$ fs) and chosen to resemble an experimental configuration [16]. The field is resonant with the $5p_{1/2}$-$5s_{1/2}$ Rb energy difference within its bandwidth at all distances $R \geqslant 8.37$ Å from the Cs atom. The potential curves of Fig. 1(a) suggest that on energetic grounds, for light-atom interactions maintained within the weak-field regime, laser light at $\lambda_0 \leqslant 662.5$ nm may be adopted for beneficial generation of molecules in vibrational levels $n_X \leqslant 20$ of the $X^1\Sigma^+$ state by stimulated emission. The *ab initio* potential curves supplied on the website of Ref. [18] and the vibrational eigenspectrum resulting from application of Le Roy's LEVEL program [21] indicate that the $n_X=0$, 1, and 2 levels of the $X^1\Sigma^+$ state could be reached by fields at wavelengths $\lambda_0=622.1$, 624.1, and 626.1 nm in the weak-field regime. Accordingly, to investigate the possibility of enhanced generation of molecules in low-lying vibrational levels of the ground electronic state, we also studied stimulated emission by a second field centered at $\lambda_0=622\pm16$ nm, contemporaneous with the field at $\lambda_0=811$ nm which serves mainly to promote photoassociation. The components of the bichromatic field so formed have equal maximum field strengths $|\boldsymbol{E}_0|=1.25\times10^{-4}$ a.u.such that its peak, frequency-integrated intensity was identical to that of the single-color field at $\lambda_0=811$ nm. The start and end times of $\mathbf{A}(t)$ were taken to be $\pm2\sigma$ so that the colliding atoms experienced the field for total durations up to 4 ps.

C. Initial conditions

We consider here photoassociation of a dilute gas of cold atoms at thermal equilibrium at a temperature $T=2$ mK, sufficiently high to allow the thermal density operator which describes the starting state to be decomposed as a sum of Gaussian wave packets [8(a),8(c)]. In the same way as other workers [8(a),8(b),8(d),10(c)], we study the time-evolution of a Gaussian wave function of the form

$$\langle R,\mathbf{r}|\Psi_0^{(0)}(t)\rangle = \exp\{-\alpha[R(t)-R_0]^2 - ik[R(t)-R_0]\} \times \phi_0(\mathbf{r};t)/R_0, \quad (8)$$

where $k=\sqrt{2m\varepsilon}$ with $\varepsilon=1.4615\times10^{-9}$ a.u. is the average wave vector corresponding to a Maxwellian distribution of velocities, $\alpha=mk_BT$ is the variance in k, and we have invoked the Born-Oppenheimer approximation to separate the nuclear wave packet from the wave function $\phi_0(\mathbf{r};t)$ of the lowest-energy electronic state of the collision pair. A justification for the representation of a thermal state subject to photoexcitation by a single Gaussian wave packet has been provided in papers by Masnou-Seeuws *et al.* [8(b),8(d),9(a)]. For these model calculations of the photoassociation dynamics, the Rb+Cs collision was started at an initial coordinate $R_0=9.1$ Å, at which distance the difference between the potential energy of the $|1\rangle$ and $|0\rangle$ electronic states matches the center frequency of a photoassociating field at 811 nm [Fig. 1(a)].

Of concern in this investigation are the relative probabilities of photon-induced association and ionization, which we refer to the zeroth-order starting state given by Eq. (8). There is no attempt to calculate absolute photoassociation rates in this work, for which it would be necessary to evaluate the sum of Gaussian wave packets which constitute the initial density at $T=2$ mK over a vastly extended grid [8(b)–8(d)]. Calculations in which α was varied by a factor of 4 and with wave packets centered about other starting coordinates up to 80 Å were found not to change the qualitative aspects of the results presented here because of the breadth of $|\Psi_0^{(0)}(t)\rangle$; we did not include nonzero angular momentum states at large R, however, which must be incorporated in a quantitative assessment of the contribution of pairs of atoms at large interatomic distances to the overall photoassociation rate [24].

III. RESULTS AND DISCUSSION

The main results of this study concern occupation probabilities of different electronic and vibrational states of Rb+Cs driven by single-color and two-color broadband fields. Particular emphasis is on schemes for formation of molecules in the ground electronic state and low-lying vibrational levels since this is a goal of current experimental work [14(b),14(e),17]. By way of a prelude to the discussion of transition probabilities, we first briefly describe the basic wave-packet motions which influence them.

A. Basic wave-packet kinematics

The nominal root-mean-square velocity of the zeroth-order wave function $\psi_0^{(0)}(R;t)$ at $T=2$ mK is $|\mathbf{v}|=4\times10^{-3}$ Å/ps, but the attractive force acting on the wave packet accelerates it up to velocities as high as $|\mathbf{v}|\simeq1.9$ Å/ps within the first oscillation period. As a result, the ground-state wave function, whether calculated to zeroth or second order, takes about 3 ps to propagate inwards to its inner turning point at $R\simeq5.1$ Å, reverse direction and return to close to its starting position at $R_0=9.1$ Å. The wave function promoted to the $(4)0^+$ potential requires a similar time to complete a single oscillation which returns it to an average distance $\langle R_1\rangle=8.3$ Å. As examples, Figs. 2(a) and 2(b) present the norms $\|\psi_1^{(1)}(R;t)\|$ and $\|\psi_0^{(2)}(R;t)\|$ at the end ($t=2\sigma=2$ ps) of a 1 ps pulse which is either unchirped or chirped to maximize $|1\rangle\leftarrow|0\rangle$ absorption according to Eq. (6). Modulating the phase of the photoassociating field changes the spatial and momentum distributions, as well as the amplitudes, of the first- and second-order wave functions in the optically connected states. Irrespective of $\phi(t)$, the wave-function amplitude becomes fragmented due to destructive interference and spreads between inner and outer turning points of the relevant potential within less than 1 ps.

The motions of the wave-packet centers are shown in Figs. 2(c) and 2(d), which plot the expectation values $\langle R_q^{(r)}\rangle(t)$ ($r=1,2$, $q=0,1$) during 1 ps photoassociation fields with different $\phi(t)$. Except when the phase of the driving field is modulated according to $d\phi(t)/dt=\Delta V_2[R(t)]-\omega_0$, the wave-function centers exhibit residual oscillatory behavior throughout the 4 ps application of the field, even though

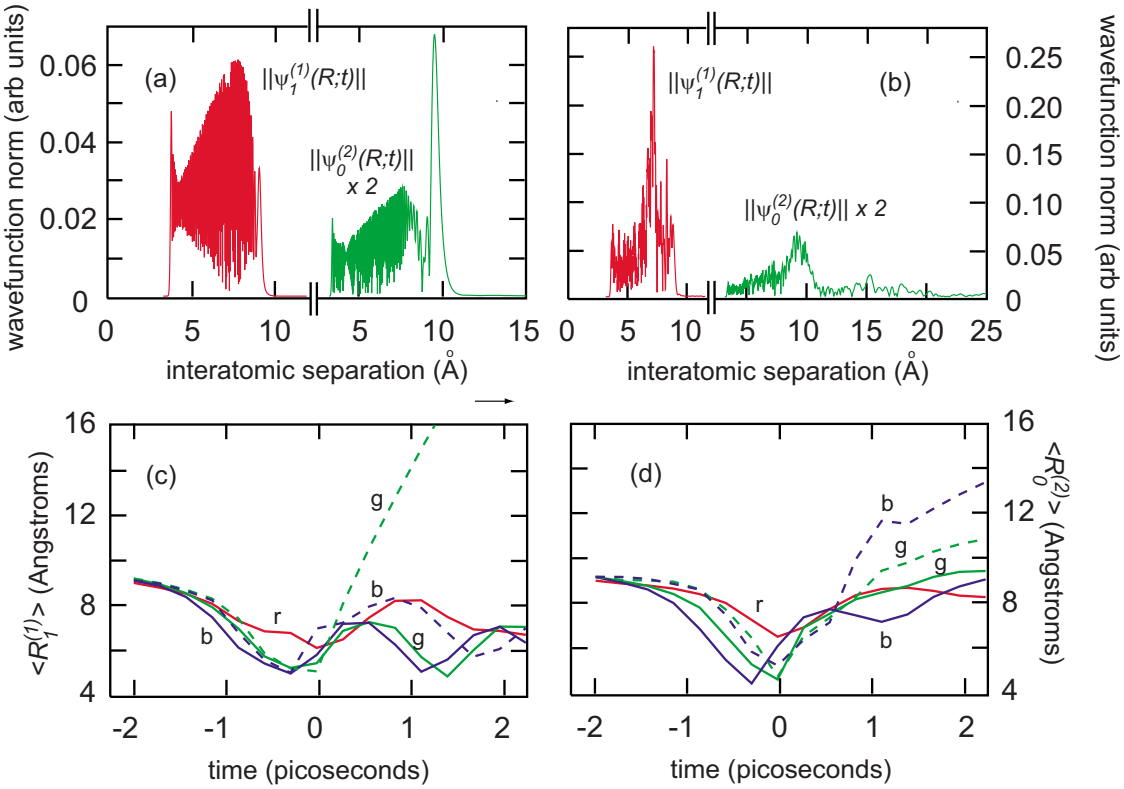

FIG. 2. (Color online) Distributions of $\|\psi_1^{(1)}(R;t)\|$ (red) and $\|\psi_0^{(2)}(R;t)\|$ (green) along the interatomic coordinate at the end ($t=2\sigma=2$ ps) of a 1 ps optical pulse. The **E** field of the pulse is either bandwidth-limited (a) or chirped to maximize $|A_{1\leftarrow 0}^{(1)}(t)|$ with $d\phi(t)/dt=\Delta V_1[\langle R_0\rangle(t)]-\omega_0$ (b). Variation of the expectation values $\langle R_1\rangle(t)=\langle\Psi_1^{(1)}(t)|R|\Psi_1^{(1)}(t)\rangle$ (c) and $\langle R_0\rangle(t)=\langle\Psi_0^{(2)}(t)|R|\Psi_0^{(2)}(t)\rangle$ (d) during a 1 ps pulse when the temporal phase of the applied **E** field is modulated by $d\phi(t)/dt=0$ (red graphs labeled "*r*"), $d\phi(t)/dt=\Delta V_1[\langle R_0\rangle(t)]-\omega_0$ and $\Delta V_2[\langle R_0\rangle(t)]-\omega_0$ (green full and dashed graphs, respectively, labeled "*g*") and $d\phi(t)/dt=\Delta V_1[\langle R_1\rangle(t)]-\omega_0$ and $\Delta V_2[\langle R_1\rangle(t)]-\omega_0$ (blue full and dashed graphs, respectively, labeled "*b*").

their amplitudes are spatially delocalized, and for at least a further 2 ps after the field is switched off (not shown). The evolution of the average separation of atom pairs which do not interact with the light field follows that of the second-order state dumped on the ground-state potential by an unchirped field, and is shown by the red-colored curve in Fig. 2(d). Figures 2(c) and 2(d) reveal that the wave-packet centers penetrate to shorter interatomic distances when the photoassociating field is chirped. The different time dependences of $\langle R_1\rangle(t)$ and $\langle R_0\rangle(t)$ suggests that the application of driving fields whose phases are modulated to maximize $|A_{1\leftarrow 0}^{(1)}(t)|$ or $|A_{1\rightarrow 0}^{(1)}(t)|$ might be expected to result in preferential population of different vibrational levels, namely those whose eigenfunctions have significant amplitude at the different turning points of the trajectories $\langle R_0\rangle(t)$ and $\langle R_1\rangle(t)$. This leads to occupation probabilities of a given vibrational quantum state which differ by up to an order of magnitude, as discussed in Sec. III C. Both wave functions $\psi_1^{(1)}(R;t)$ and $\psi_0^{(2)}(R;t)$ spread faster than their centers move at $T=2$ mK; their distribution across the potential wells of the optically connected states, coupled with the steep variation of the magnitude of the Franck Condon factors [Figs. 1(b)], acts to mask the sharper differences in population of a given vibrational level which would otherwise result from application of driving fields with different temporal phase modulations.

Figures 2(a) and 2(b) indicate that the excited-state amplitude $\psi_1^{(1)}(R;t)$ remains bound at $R\leqslant 10$ Å for all $t\leqslant 2$ ps when excited-state amplitude is promoted by a field which is transform limited or phase modulated by $\Delta V_1[\langle R_0\rangle(t)]$. Figure 2(c) reveals, by contrast, that modulating the temporal phase by $\Delta V_2[\langle R_0\rangle(t)]$ to optimize $|1\rangle\leftarrow|0\rangle$ absorption substantially enhances the dissociative component of $\psi_1^{(1)}(R;t)$ at $R>10$ Å and hence leads to loss of incipient molecules. The difference between phase modulations given by Eqs. (6) and (7) is not so pronounced when the applied field is chirped to optimize $|1\rangle\rightarrow|0\rangle$ emission, but more $\psi_0^{(2)}(R;t)$ nevertheless proceeds to redissociation along the ground-state asymptote. From calculated values of $|A_{0\leftarrow 0}^{(2)}(t)|^2$ we find redissociated fractions $\|\psi_0^{(2)}(R>10\text{ Å};t)\|^2/\|\psi_0^{(2)}(R;t)\|^2$ of 0.21 and 0.32 at $t=2$ ps when the phase of the driving field is tailored to photon absorption according to Eqs. (6) and (7), respectively; likewise, $\|\psi_0^{(2)}(R>10\text{ Å};t)\|^2/\|\psi_0^{(2)}(R;t)\|^2=0.15$ and 0.34 when the temporal phase promotes stimulated emission according to Eqs. (6) and (7). For a transform-limited field, the fractional dissociation of initial population at 2 ps is 0.01 and in the absence of any interaction with light it is 0.001. The principal finding of Fig. 2 is that application of positively chirped fields to Rb+Cs collisions brings about greater dissociation to separated atoms, rather than their association, compared to negatively chirped fields.

B. Electronic state populations

Figures 3(a) and 3(b) compare the probabilities $\|\psi_1^{(1)}(R\leqslant 10\text{ Å};t)\|^2$ and $\|\psi_0^{(2)}(R\leqslant 10\text{ Å};t)\|^2$ of occupation of the

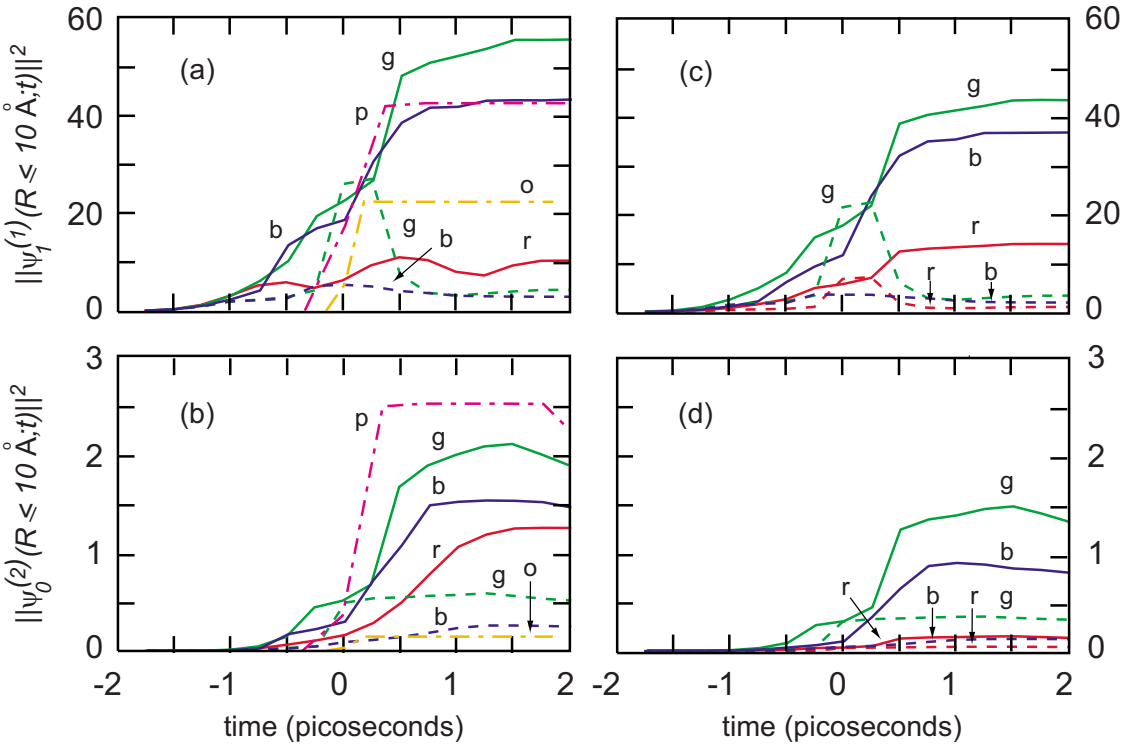

FIG. 3. (Color online) Probabilities $\|\psi_1^{(1)}(R\leqslant 10\ \text{Å};t)\|^2$ [(a) and (c)] and $\|\psi_0^{(2)}(R\leqslant 10\ \text{Å};t)\|^2$ [(b) and (d)] of occupation of the bound portions of the $X^1\Sigma^+$ and $3^1\Sigma^+$ states of RbCs at $R\leqslant 10$ Å as a function of time. Graphs (a) and (b) show results for a single-color field at $\lambda_0=811$ nm, of maximum field strength $|\mathbf{E}_0|=2.5\times10^{-4}$ a.u. and duration $\sigma=1$ ps unless otherwise stated, and with different phase modulations color coded as follows: $d\phi(t)/dt=0$ (red); $\Delta V_1[\langle R_0\rangle(t)]-\omega_0$ (green); $\Delta V_1[\langle R_1\rangle(t)]-\omega_0$ (blue); $\Delta V_2[\langle R_0\rangle(t)]-\omega_0$ (green dashed); $\Delta V_2[\langle R_1\rangle(t)]-\omega_0$ (blue dashed); $-2.2184\times10^{-4}t/[\text{fs}]$ rad/fs with $\sigma=355$ fs (purple dotted-dashed); $4.7029\times10^{-4}t/[\text{fs}]$ rad/fs with $\sigma=167$ fs (orange dotted-dashed). Graphs (c) and (d) compare probabilities excited by a 1 ps bichromatic field with $|\mathbf{E}_0|=2.5\times10^{-4}$ a.u. and temporally overlapped components at $\lambda_0=811$ and 622 nm. The fields are phase-modulated according to the color code: $d\phi_{622}(t)/dt=0$ and $d\phi_{811}(t)/dt=\Delta V_1[\langle R_0\rangle(t)]-\omega_0$ (red); $d\phi_{622}(t)/dt=d\phi_{811}(t)/dt=\Delta V_1[\langle R_0\rangle(t)]-\omega_0$ (green); $d\phi_{622}(t)/dt=\Delta V_1[\langle R_1\rangle(t)]-\omega_0$ and $d\phi_{811}(t)/dt=\Delta V_1[\langle R_0\rangle(t)]-\omega_0$ (blue); $d\phi_{622}(t)/dt=0$ and $d\phi_{811}(t)/dt=\Delta V_2[\langle R_0\rangle(t)]-\omega_0$ (red dashed); $d\phi_{622}(t)/dt=d\phi_{811}(t)/dt=\Delta V_2[\langle R_0\rangle(t)]-\omega_0$ (green dashed); $d\phi_{622}(t)/dt=\Delta V_2[\langle R_1\rangle(t)]-\omega_0$ and $d\phi_{811}(t)/dt=\Delta V_2[\langle R_0\rangle(t)]-\omega_0$ (blue dashed). Red, green, blue, purple, and orange graphs are labeled "*r*," "*g*," "*b*," "*p*," and "*o*," respectively. Values of $\|\psi_1^{(1)}(R\leqslant 10\ \text{Å};t)\|^2$ and $\|\psi_0^{(2)}(R\leqslant 10\ \text{Å};t)\|^2$ are normalized with respect to the zeroth-order transition probability $|U_0^{(0)}(t,t_0)|^2=1$ at $t=2\sigma$ with $t_0=-2\sigma$.

bound regions of $|1\rangle$ and $|0\rangle$ at $R\leqslant 10$ Å derived from $|A^{(1)}_{1\leftarrow0}(t)|^2$ and $|A^{(2)}_{0\leftarrow0}(t)|^2$ under different conditions of chirp applied to the photoassociating field. We see that the field chosen to maximize $|1\rangle\leftarrow|0\rangle$ single-photon absorption by means of a phase modulated by the classical potential energy difference offers the best possibility for maximizing excited-state population at bound interatomic separations [green curve in Fig. 3(a)]: compared to that generated by a bandwidth-limited pulse, chirping the field in this way enhances $\|\psi_1^{(1)}(R\leqslant 10\ \text{Å};t)\|^2$ by a factor of 5.4 at $t=2\sigma$. Phase modulations which seek to maximize $|1\rangle\leftrightarrow|0\rangle$ absorption or emission in accord with $V_1(R_0)-V_0[\langle R_q\rangle(t)]$ result in a time dependence of $\|\psi_1^{(1)}(R\leqslant 10\ \text{Å};t)\|^2$ which mimics the envelope intensity profile of the driving field and which thereby restricts the temporal opportunity for transfer of population between $|0\rangle$ and $|1\rangle$ at bound configurations. In contrast to the excited state, the second-order population in the ground state at $R\leqslant 10$ Å is maximized along the trailing edge of a linearly down-chirped pulse of 355 fs duration [purple doted-dashed graph in Fig. 3(b)], which marginally outperforms a 1 ps pulse whose temporal phase is modulated by $\Delta V_1[\langle R_1\rangle(t)]$ to enhance $|1\rangle\leftarrow|0\rangle$ absorption (green curve). Driving fields whose temporal phases are matched to either $\Delta V_1[\langle R_1\rangle(t)]$ or $\Delta V_2[\langle R_1\rangle(t)]$ to maximize $|1\rangle\rightarrow|0\rangle$ stimulated emission do not result in a maximal number of molecules in the $X^1\Sigma^+$ state within a two-level representation of Rb+Cs. Values of $\|\psi_0^{(2)}(R\leqslant 10\ \text{Å};t)\|^2$ decrease at $t>1.5$ ps when the phase of the applied field is down chirped, either linearly or by $\Delta V_1[\langle R_1\rangle(t)]$. That $|A^{(2)}_{0\leftarrow0}(t)|^2$ is maximized when negatively chirped and absorption-matched fields are applied to the colliding atoms indicates that it is more expedient to generate maximal population in the excited electronic state for subsequent, nonoptimized, stimulated emission, than it is to maximize the probability of $|1\rangle\rightarrow|0\rangle$ stimulated emission pumping from a $3^1\Sigma^+$ population generated beforehand by a field not optimally adapted for its prior availability.

Even though fields whose temporal phase is modulated by $\Delta V_1[\langle R_0\rangle(t)]$ to maximize $A^{(1)}_{1\leftarrow0}(t=2\sigma)$ results in a greater probability of atomic redissociation along the asymptote of $|0\rangle$ [Fig. 2(b)] compared to linearly chirped fields, such fields remain optimal for production of bound atomic pairs at $R\leqslant 10$ Å in the ground electronic state. The ratios of second-order probabilities $|A^{(2)}_{0\leftarrow0}(t)|^2$ pertaining at the end of 1 ps pulses are 1.5:1.2:1.0 when $d\phi(t)/dt+\omega_0=\Delta V_1[\langle R_0\rangle(t)]$,

$\Delta V_1[\langle R_1\rangle(t)]$, and ω_0, respectively, and 0.4:0.2:1.0 when $d\phi(t)/dt+\omega_0=\Delta V_2[\langle R_0\rangle(t)]$, $\Delta V_2[\langle R_1\rangle(t)]$, and ω_0; the corresponding ratios (referred to $|A^{(2)}_{0\leftarrow 0}(t)|^2$ resulting from a transform-limited field) when $\phi(t)$ is linearly red chirped with $\sigma=355$ fs and linearly blue chirped with $\sigma=167$ fs are 1.7:1.0 and 0.1:1.0, respectively. The maximum fractional number of ground-state molecules generated by pump-dump transitions starting from a Gaussian wave packet located at 9.1 Å is $|A^{(2)}_{0\leftarrow 0}(t)|^2/|U_0(t,t_0)|^2=3.3\times 10^{-4}$ at $t=2\sigma$, taking into account recollisional loss of atoms which have interacted with light. Additional calculations indicate that this result is an order of magnitude smaller than the fractional number of bound molecules created in the $X^1\Sigma^+$ state when the same fields are applied to an initial state chosen from high-lying vibrational eigenfunctions supported by the $X^1\Sigma^+$ potential such as can be generated in ultracold heteronuclear molecules at Feshbach resonances [12,25].

It is clear from Figs. 3(a) and 3(b) that the driving fields whose phases are modulated with respect to the classical difference potential $\Delta V_1[R(t)]$ outperform those whose phases are modulated by $\Delta V_2[R(t)]$ insofar as maximizing $A^{(1)}_{1\leftarrow 0}(t)$ and $A^{(2)}_{0\leftarrow 0}(t)$ is concerned. Likewise, fields with linear negative chirps result in higher values of $A^{(1)}_{1\leftarrow 0}(t)$ and $A^{(2)}_{0\leftarrow 0}(t)$ at $t=2\sigma$ than do fields with linear positive chirps. Although only one example of the probability dynamics generated by linearly chirped fields of each sign is shown in Figs. 3(a) and 3(b), similar results were obtained with fields with the same values of β/σ^2 and different values of σ (see Sec. II B): in particular, fields with linear negative chirps returned values of $|A^{(1)}_{1\leftarrow 0}(t)|^2$ and $|A^{(2)}_{0\leftarrow 0}(t)|^2$ which differ at most by 1.4 ± 0.1 at $t=2\sigma$.

Relative to the effect of a transform-limited field and the fraction of bound atomic pairs which form without interacting with the applied light field, Figs. 2 and 3 indicate that, within the remits of the two-level model of Rb+Cs and weak-field light-atom interaction regime adopted here, application of driving fields bearing a temporal phase modulation given by Eq. (7), or which carry a linear positive chirp, leads to a reduction in the number of atomic pairs formed at $R\leqslant 10$ Å. This result stands in qualitative agreement with the outcome of recent experiments in which application of a modulated light field to collisions of Rb atoms was observed to have a pernicious effect on molecule production [14], and specifically ties in with the detrimental effect of a positively chirped field reported by Brown, Dicks, and Walmsley [14(a)]. The variation of $\langle R_1\rangle(t)$ shown in Fig. 3(c) and $\langle R_2\rangle(t)$ shown in Fig. 3(d) for phase-modulated driving fields hints at the origin of the suppression of molecule generation under these chirp conditions, but the robustness of this conclusion needs to be tested by calculations of absolute photoassociation rates of Rb+Cs driven by fields with different phase modulations; such calculations are currently underway and will be presented in a future report.

That driving fields bearing the chirp $d\phi(t)/dt=\Delta V_1[R(t)]-\omega_0$ result in similar increases in $|A^{(1)}_{1\leftarrow 0}(t)|^2$ and $|A^{(2)}_{0\leftarrow 0}(t)|^2$ as a function of time to that obtained with linearly down-chirped fields suggests that matching $\phi(t)$ to the classical difference potential results in fields which are chirped predominantly to the red of ω_0. Driving fields chirped by $d\phi(t)/dt=\Delta V_2[R(t)]-\omega_0$ are anticipated to exhibit a larger

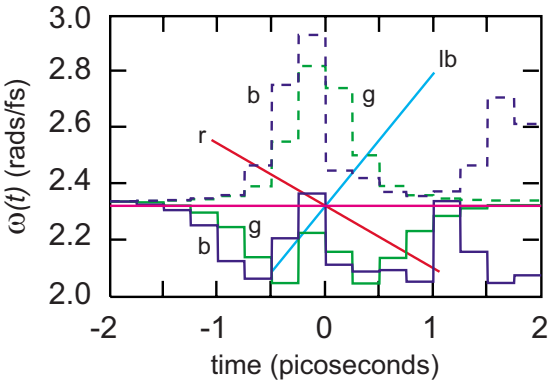

FIG. 4. (Color online) Time dependence of the local frequency $\omega(t)$ of fields resulting in the population dynamics of Fig. 3 with chirps color-coded as follows: $d\phi(t)/dt=\Delta V_1[\langle R_0\rangle(t)]-\omega_0$ (green); $\Delta V_1[\langle R_1\rangle(t)]-\omega_0$ (blue); $\Delta V_2[\langle R_0\rangle(t)]-\omega_0$ (green dashed); $\Delta V_2[\langle R_1\rangle(t)]-\omega_0$ (blue dashed); $-2.2184\times 10^{-4}t/[\text{fs}]$ (red); $4.7029\times 10^{-4}t/[\text{fs}]$ rad/fs (light blue). Red, green, blue, and light blue graphs are labelled "*r*," "*g*," "*b*," and "lb," respectively. The horizontal (purple) line indicates $\omega_0=2.3226$ rad/fs ($\lambda_0=811$ nm).

departure to the blue of ω_0 on the basis of the potential energy curve shown in Fig. 1(a). These speculations are confirmed in Fig. 4, which plots the local frequency $\omega(t)=d\phi(t)/dt$ as a function of time for the fields whose temporal phases result in the population dynamics displayed in Fig. 3. The significant increases in $|A^{(1)}_{1\leftarrow 0}(t)|^2$ and $|A^{(2)}_{0\leftarrow 0}(t)|^2$ at times near the temporal centers of driving fields with the phase modulations $\int_{-\infty}^{t}\{\Delta V_1[R(t')]-\omega_0\}dt'$ and $-\beta t^2/\sigma^2$ shown in Figs. 3(a) and 3(b), coupled with the wave-packet dynamics shown in Figs. 2(c) and 2(d), suggests that down chirping acts most effectively in transferring amplitude between electronic states during outwards-bound motion of $\psi^{(1)}_1(R;t)$ and $\psi^{(2)}_0(R;t)$ between $R\simeq 5.1$ and 7.5 Å rather than on an inwards-bound trajectory from 9.1 Å for which it was obstensibly designed.

Figures 3(c) and 3(d) compare values of $\|\psi^{(1)}_1(R\leqslant 10\ \text{Å};t)\|^2$ and $\|\psi^{(2)}_0(R\leqslant 10\ \text{Å};t)\|^2$ promoted by bichromatic fields whose components at $\lambda_0=811$ and 622 nm have field strengths $|\mathbf{E}_0|=1.25\times 10^{-4}$ a.u.; the temporal phase of the 811 nm field is chirped to maximize stimulated absorption according to Eq. (6). If $A^{(1)}_{1\leftarrow 0}(t)$ and $A^{(2)}_{0\leftarrow 0}(t)$ were determined solely by the long-wavelength field component, a decrease in $|A^{(1)}_{1\leftarrow 0}(t)|^2$ by a factor of 4 and in $|A^{(2)}_{0\leftarrow 0}(t)|^2$ by a factor of 16 would be expected when its field strength is halved. Such reductions are confirmed quantitatively in Figs. 3(c) and 3(d) in the case that the 622 nm field remains transform-limited (red curves). When the phases of both components are modulated by $\Delta V_1[R(t)]$, the bichromatic field is relatively more efficient than the single-color field at generating bound atomic pairs in the excited state by factors of 3.1 (green curve) and 2.7 (blue curve) and in the ground state by factors of 11 (green curve) and 8.7 (blue curve). These results demonstrate that the shorter-wavelength component of a bichromatic field, although initially far off resonance with transitions of the separated atoms, plays a substantial role in $|1\rangle\rightarrow|0\rangle$ stimulated emission, even when its temporal phase is matched to $\Delta V_1[\langle R_0\rangle(t)]$ rather than

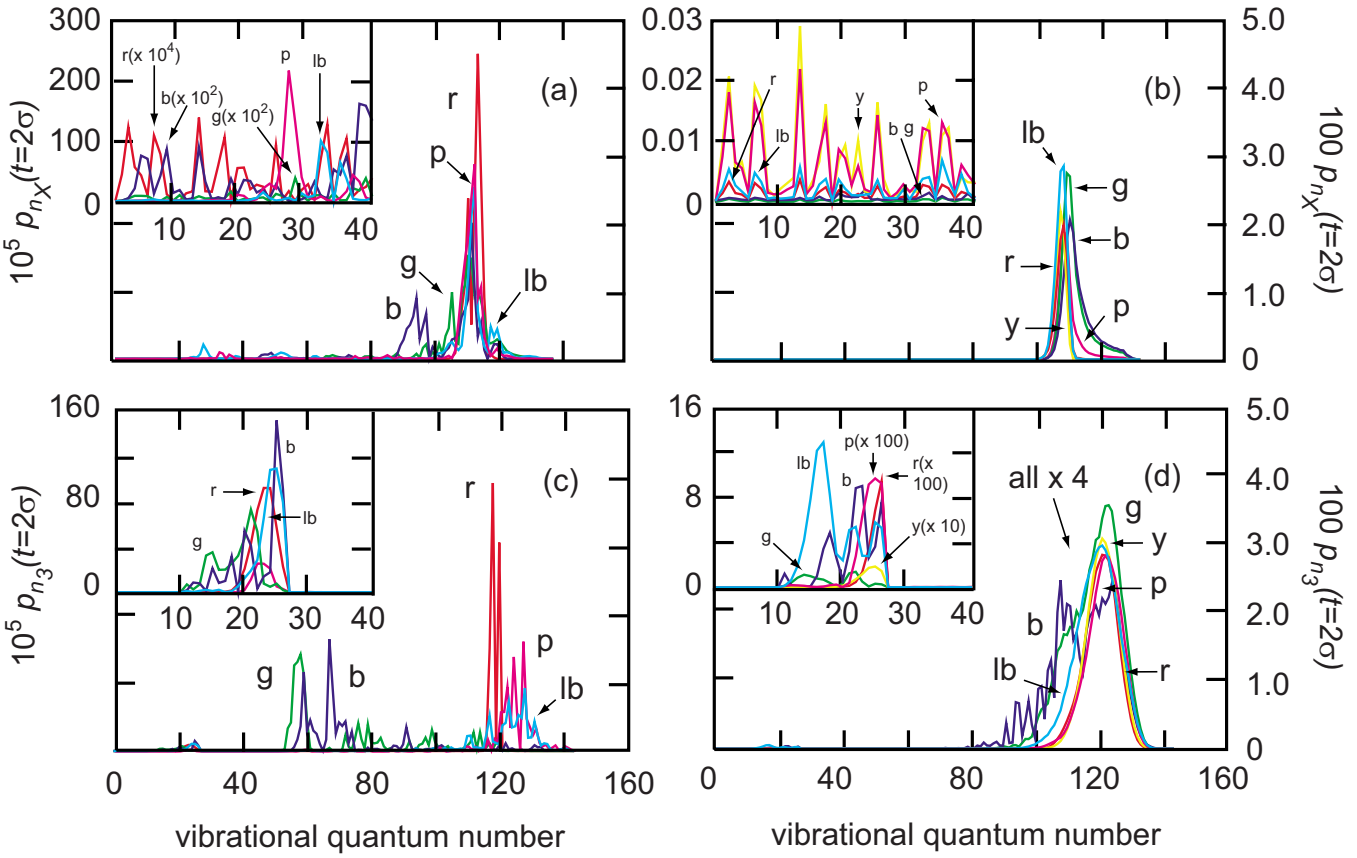

FIG. 5. (Color online) Probabilities $p_{n_X}(t=2\sigma)$ and $p_{n_3}(t=2\sigma)$ of vibrational levels supported by the $X^1\Sigma^+$ [(a) and (b)] and $3^1\Sigma^+$ [(c) and (d)] potential wells at the end of a chirped field of maximum strength $|\mathbf{E}_0|=2.5\times10^{-4}$ a.u. at $\lambda_0=811$ nm. Graphs (a) and (c) show probability distributions derived from 1 ps fields with chirps $d\phi(t)/dt=0$ (red), $\Delta V_1[\langle R_0\rangle(t)]-\omega_0$ (green), $\Delta V_1[\langle R_1\rangle(t)]-\omega_0$ (blue), $\Delta V_2[\langle R_0\rangle(t)]-\omega_0$ (purple), and $\Delta V_2[\langle R_0\rangle(t)]-\omega_0$ (light blue). Graphs (b) and (d) show probability distributions obtaining from linearly down-chirped Gaussian fields with $d\phi(t)/dt=-2.2184\times10^{-4}t/[\text{fs}]$ rad/fs and $\sigma=175$ fs (red), $\sigma=355$ fs (green), and $\sigma=530$ fs (dark blue) and from linearly up-chirped Gaussian fields with $d\phi(t)/dt=4.7029\times10^{-4}t/[\text{fs}]$ rad/fs and $\sigma=83$ fs (yellow), $\sigma=167$ fs (purple) and $\sigma=250$ fs (light blue). The main body of each diagram shows $p_{n_{X(3)}}(t=2\sigma)$ for all vibrational levels with values indicated by the scale on the right-hand ordinate; the inset to each diagram magnifies $p_{n_{X(3)}}(t=2\sigma)$ between $n_{X(3)}=0$ and 40 with values shown by the scale of the left-hand ordinate. In the inset to (a), the red spectrum is multiplied by 10^4 and the green and blue spectra by 100; in the main part of (d), all $p_{n_3}(t=2\sigma)$ are multiplied by 4 and in the inset to (d), the yellow spectrum is multiplied by 10 and the red and purple spectra by 100. Graphs labeled "*r*," "*g*," "*b*," "*p*," "lb," and "*y*" designate red, green, blue, purple, light blue, and yellow, respectively.

$\Delta V_1[\langle R_1\rangle(t)]$. Figures 3(c) and 3(d) also indicate the desirability of phase modulating $\mathbf{E}(t)$ by the classical potential energy difference $\Delta V_1[R(t)]$ rather than $V_1(R_0)-V_1[R(t)]$ when the goal is to generate a maximal number of molecules at $R\leqslant 10$ Å at the end of the pulse.

C. Vibrational level distributions

Occupation probabilities of the divers vibrational levels $|n\rangle$ supported by the potential wells of the optically connected electronic states were calculated from $p_n(t)=|\langle n|\Psi_q^{(r)}(t)\rangle|^2$ subject to the normalization condition $\Sigma_n\Sigma_t p_n(t)=1$. Vibrational eigenfunctions were computed using Le Roy's LEVEL 8.0 program [21] with the *ab initio* potential functions of Ref. [18] as input. The calculated maximum number of vibrational levels supported by the potential wells of the $X^1\Sigma^+$ and $3^1\Sigma^+$ electronic states is respectively 136 and 144. Figure 5 compares the probabilities $p_{n_X}(t=2\sigma)$ and $p_{n_3}(t=2\sigma)$ of occupancy of the vibrational levels of the $X^1\Sigma^+$ and $3^1\Sigma^+$ electronic states at the end of a driving field centered at 811 nm with different temporal phases. The principal characteristics of the distributions are a transform-limited driving field leads to a sharp distribution of probability clustered about $n_X=112$ in the $X^1\Sigma^+$ state and $n_3=118$ in the $3^1\Sigma^+$ state; and transitions to more deeply bound oscillator levels become non-negligibly probable compared to their largest values delivered by the Fourier pulse only when the temporal phase of the driving field is matched to $\Delta V_1[R(t)]$ or $\Delta V_2[R(t)]$. Differences in $p_{n_X}(t=2\sigma)$ and $p_{n_3}(t=2\sigma)$ generated by different chirped fields are not as marked. The inset to Fig. 5(a) reveals that the probability of transitions to (desirable) low-lying levels of the $X^1\Sigma^+$ state with $n_X\leqslant 40$ is greatest when the temporal phase of the driving field is modulated by $\Delta V_2[R(t)]$ according to Eq. (7), and that the replacements $R(t)\rightarrow\langle R_1\rangle(t)$ or $\langle R_0\rangle(t)$ to optimize stimulated emission or absorption respectively facilitate preferential population of different low-lying oscillator levels: values of $p_{n_X}(t=2\sigma)$ for $3\leqslant n_X\leqslant 40$ remain on the

TABLE I. Probabilities $P_{n_{X(3)}}(t=2\sigma)$ per pair of colliding atoms of generating RbCs molecules in selected vibrational levels n_X and n_3 of the $X^1\Sigma^+$ and $3^1\Sigma^+$ states at the end ($t=2\sigma$) of single-color and bichromatic driving fields of maximum amplitude $|\mathbf{E}_0|=2.5\times10^{-4}$ a.u., duration $\sigma=1$ ps, and different temporal phases. For the bichromatic field, the different $\phi(t)$ pertain to the 622 nm field when the 811 nm component is chirped to maximize $|1\rangle\leftarrow|0\rangle$ absorption according to Eq. (6).

	$X^1\Sigma^+$ state		$3^1\Sigma^+$ state	
$d\phi(t)/dt+\omega_0$	n_X	$10^4P_{n_X}(t=2\sigma)$	n_3	$10^4P_{n_3}(t=2\sigma)$
Single-color field, $\lambda_0=811$ nm				
ω_0	112	3.6	118	44
	0	9.7×10^{-8}		
$\Delta V_1[\langle R_1\rangle(t)]$	110	2.5	67	68
	13	1.1×10^{-3}		
	0	1.1×10^{-6}		
$\Delta V_1[\langle R_0\rangle(t)]$	109	2.5	58	67
	0	9.7×10^{-7}		
$\Delta V_2[\langle R_1\rangle(t)]$	111	0.75	126	5.0
	23	3.8×10^{-3}		
	0	8.1×10^{-6}		
$\Delta V_2[\langle R_0\rangle(t)]$	111	1.5	127	4.9
	0	2.0×10^{-6}		
Bichromatic field, $\lambda_0=811/622$ nm				
ω_0	110	0.05	123	4.1
	0	2.4×10^{-7}		
$\Delta V_1[\langle R_1\rangle(t)]$	112	1.3	127	27
	11	4.2×10^{-4}		
	0	8.8×10^{-8}		
$\Delta V_1[\langle R_0\rangle(t)]$	109	1.9	125	17
	0	1.1×10^{-6}		

order of 10^{-3} of the total probability at $t=2\sigma$, however. Irrespective of the modulation applied to the driving field, the occupation probabilities between $n_X=$and 40 vary at most by an order of magnitude between neighboring levels, which is much smaller than the variation of more than ten orders of magnitude in Franck-Condon factors for transitions across the same energy range accessed by a transform-limited field [Fig. 1(b)]. The locations of the maxima and minima in $p_{n_X}(t=2\sigma)$ do not correspond to differences between Franck-Condon factors for transitions to different n_X levels.

To gain a quantitative idea of the relative numbers of bound molecules generated in specific oscillator levels by broadband photoassociation of a given starting state under weak-field conditions, Table I lists selected probabilities $P_{n_{X(3)}}(t)$ at $t=2\sigma$ renormalized with respect to the probabilities for transitions between electronic states, themselves referenced to the zeroth-order transition probability $|U_0^{(0)}(t,t_0)|^2$, i.e., $P_{n_X}(t)=p_{n_X}(t)|A^{(2)}_{0\leftarrow0}(t)|^2$ and $P_{n_3}(t)=p_{n_3}(t)|A^{(1)}_{1\leftarrow0}(t)|^2$. For the most populated levels of the $X^1\Sigma^+$ and $3^1\Sigma^+$ states with $n_X>100$ and $n_3>50$, the fractional occupation probabilities are $P_{n_X}(t=2\sigma)\simeq10^{-4}$ and $P_{n_3}(t=2\sigma)\simeq10^{-3}$. Because the production of ultracold polar molecules in deeply bound levels is of current experimental interest [12,14(b),14(e),17], Table I also reports the probability of generating $X^1\Sigma^+$ molecules in the zero-point and selected deeply-bound oscillator levels. Although its application to a single-color field at 811 nm results in fewer molecules overall, the phase modulation of Eq. (7) in which $\phi(t)$ is referred to the shape of $V_0(R)$ generates amplitude in the zero-point level with probabilities 2.1 and 7.5 times higher than those achieved when $\phi(t)$ is modulated by the classical difference potential to optimize absorption and stimulated emission, respectively. The same observation is qualitatively applicable to the probabilities of all levels $n_X\leqslant40$ achieved by the different phase modulations investigated here.

Figure 6 displays the different temporal profiles $p_{n_X}(t)$ and $p_{n_3}(t)$ exhibited by oscillator levels of the $X^1\Sigma^+$ and $3^1\Sigma^+$ states which yield high and low probabilities at $t=2\sigma$. Here, values of $p_{n_X}(t)$ and $p_{n_3}(t)$ deriving from fields modulated by the classical difference potentials and a linear down chirp are presented with those pertaining to a transform-limited field, these data being representative of the time-dependent behaviors of different $p_{n_X}(t)$ and $p_{n_3}(t)$ obtained from all the phase-modulated fields investigated in this work. Vibrational levels with the highest occupation probabilities at $t=2\sigma$ display a time dependence, depicted by the filled curves in Fig. 6, which broadly resembles that of the electronic transition probabilities $|A^{(1)}_{1\leftarrow0}(t)|^2$ and $|A^{(2)}_{0\leftarrow0}(t)|^2$ shown in Fig. 3. Unfavorably populated levels, by contrast, exhibit a growth and decay behavior during the evolution of the field as exemplified by the dashed curves in Fig. 6. The location of temporal maxima in $p_n(t)$ reflects the changing position of the main peaks of $\psi_0^{(2)}(R;t)$ and $\psi_1^{(1)}(R;t)$ with respect to the interatomic separations over which the spectral bandwidth maps onto the potential energy curves, as well as the intensity profile of the pulse and the Franck-Condon factors pertaining to overlap of specific vibrational eigenfunctions.

The results of Fig. 5 together with the values of $P_{n_X}(t=2\sigma)$ listed in Table I suggest that a field of shorter wavelength might be beneficially employed to generate molecules in more deeply bound vibrational levels of the ground electronic state by stimulated emission of a single photon while maintaining weak-field conditions. To investigate this possibility, we carried out calculations in which a 1 ps field at $\lambda_0=811$ nm, providing photons primarily for $|1\rangle\leftarrow|0\rangle$ absorption, was temporally overlapped with a second field of the same duration and different bandwidths centered at $\lambda_0=622$ nm, primarily to stimulate emission to the $n_X=0-3$ levels of the $X^1\Sigma^+$ state. The maximum field strength of the two components was selected to be $|\mathbf{E}_0|=1.25\times10^{-4}$ a.u. so that the bichromatic field presented the same on-target maximum intensity (integrated over frequency) as the single-color field at $\lambda_0=811$ nm considered above. Given a center wavelength, the choice of bandwidth of the additional field depends on whether spectral or temporal resolution is required: the former allows selection of individual vibrational levels; the latter allows precise control of the temporal adjustment of the two fields and hence of ground-state molecule formation. Here, the effect of different bandwidths on the transition amplitudes for stimulated emission was investigated by applying different chirps to the phase $\phi_{622}(t)$ of the 622 nm field.

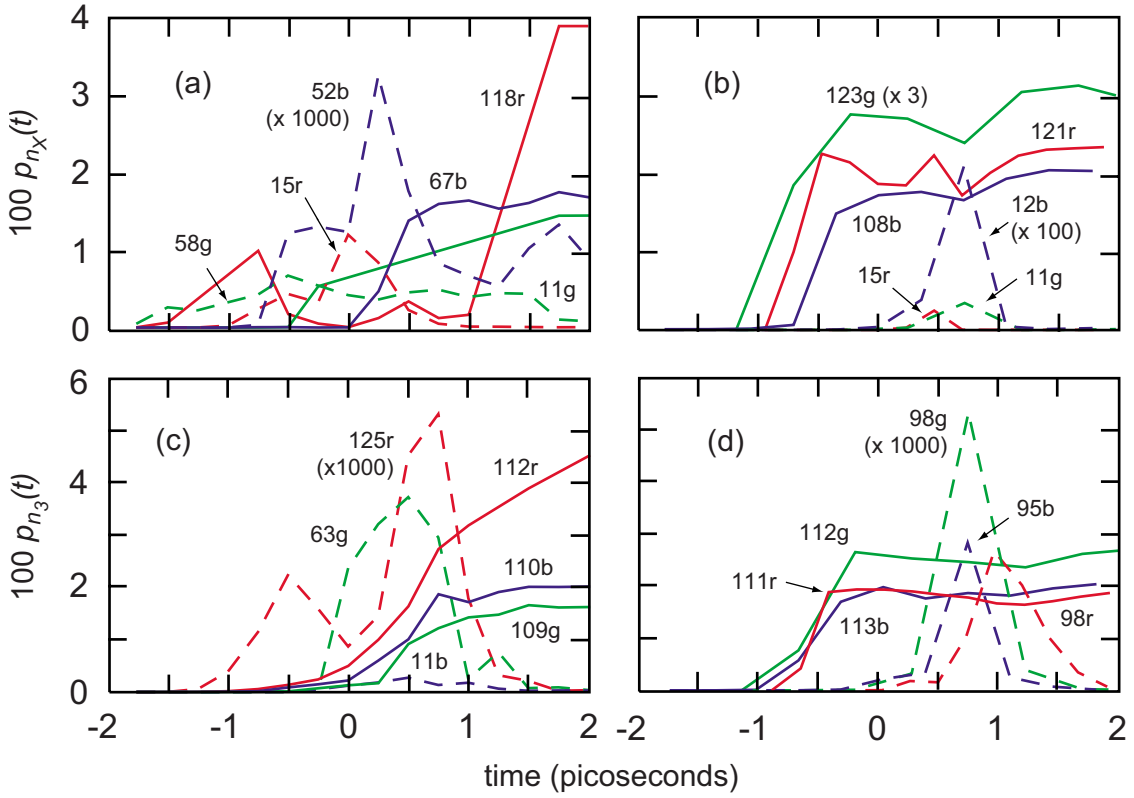

FIG. 6. (Color online) Probabilities $p_{n_X}(t)$ and $p_{n_3}(t)$ as a function of time for vibrational levels n_X and n_3 supported by the potential wells of the $X^1\Sigma^+$ state [(a) and (b)] and $3^1\Sigma^+$ state [(c) and (d)] driven by a field of maximum amplitude $|\mathbf{E}_0|=2.5\times10^{-4}$ a.u. subject to different phase modulations. Red, green, and blue curves in graphs (a) and (c) display $p_{n_X}(t)$ and $p_{n_3}(t)$ promoted by 1 ps fields with $d\phi(t)/dt=0$, $\Delta V_1[\langle R_0\rangle(t)]-\omega_0$ (absorption optimized) and $d\phi(t)/dt=\Delta V_1[\langle R_1\rangle(t)]-\omega_0$ (stimulated emission optimized), respectively. Graphs (b) and (d) show $p_{n_X}(t)$ and $p_{n_3}(t)$ obtaining from linearly down-chirped Gaussian fields with $d\phi(t)/dt=-2.2184\times10^{-4}t/[\text{fs}]$ rad/fs and durations $\sigma=175$ (red curves), 355 (blue curves), and 530 (green curves) fs, respectively. The labels near each curve comprise values of n_X and n_3, "r," "g," or "b" to designate red, green, and blue in accordance the color scheme given above and, where appropriate, multiplication factors applied to $p_{n_X}(t)$ and $p_{n_3}(t)$ in parentheses. The filled and dashed curves indicate the two principal types of time dependence (see text).

Plotted in Fig. 7 are vibrational level occupation probabilities as a function of quantum number obtaining at the end of a 1 ps bichromatic field in which $\phi_{622}(t)$ is either constant (zero) or chirped to maximize $A^{(1)}_{1\leftarrow0}(t)$ or $A^{(2)}_{0\leftarrow0}(t)$ by modulating $\phi(t)$ in terms of the classical difference potential [Eq. (6)]; the phase $\phi_{811}(t)$ of the near infrared field was chirped to maximize the probability of $|1\rangle\leftarrow|0\rangle$ absorption according to Eq. (6). The variation of $p_n(t)$ with time for different n_X and n_3 driven by a bichromatic field displays the same qualitative aspects as those shown in Fig. 6 for excitation by a single-color field. Inspection of the ordinates of Figs. 5 and 7 indicates that the addition of a shorter-wavelength component to the driving field, while maintaining the same on-target field strength, redistributes probability between vibrational levels, but does not result in a substantial (say, by more than an order of magnitude) accumulation of population into different levels compared to that achieved by the single-color field at 811 nm. The probability of deeply bound levels $0\leqslant n_X\leqslant10$ increases by a factor of 10 when Rb+Cs is photoassociated by a bichromatic field, with the one exception of the zero-point level, for which Table I indicates that the occupation probability increases by a factor of 2.5 when $\phi_{622}(t)$ is constant and decreases when $\phi_{622}(t)$ is modulated: values of $P_{n_X=0}(t=2\sigma)$ range from 8.8×10^{-12} to 1.1×10^{-10} relative to the zeroth-order wave packet.

D. Ionization

Owing to the high peak intensities of femto- and picosecond laser pulses and the (relatively low) ionization potentials of the target alkali-metal atoms, ionization by the field employed for RbCs photoassociation is considered likely a concern in experiments where ionization is planned for state- or time-resolved detection of bound atomic pairs, as in experiments with homonuclear molecular targets [23]. Within the three-state model adopted here, direct three-photon ionization from the ground $(1)0^+$ state and $(1+2)$-photon resonant ionization via the intermediate $|1\rangle$ state are energetically feasible with incident light at $\lambda_0=811$ nm under weak-field conditions. When light at $\lambda_0=622$ nm is applied to Rb+Cs collisions, one less photon is required for ionization via the same channels. The vertical arrows displayed in Fig. 1(a) illustrate the various ionization routes. To investigate the situation where ionization is likely to be most dominant, in this section we compare the probabilities of ionization induced by fields whose phase is modulated according to Eq.

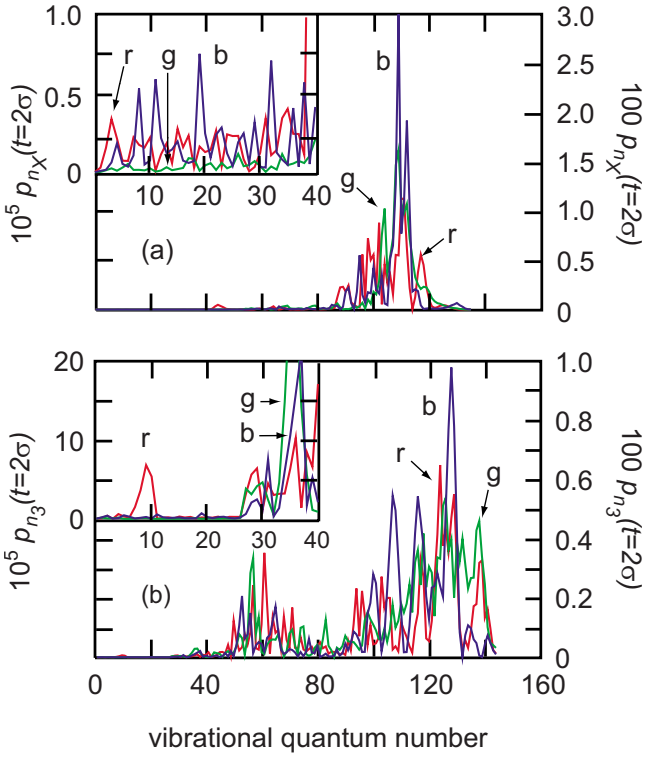

FIG. 7. (Color online) Probability distributions $p_{n_X}(t=2\sigma)$ and $p_{n_3}(t=2\sigma)$ for transitions to vibrational levels of the $X^1\Sigma^+$ state (a) and $3^1\Sigma^+$ state (b) at the end ($t=2\sigma$) of a bichromatic field with components centered at 811 and 622 nm and maximum amplitudes $|\mathbf{E}_0|=1.25\times10^{-4}$ a.u. The 622 nm component is either transform limited (red graphs) or phase modulated according to $d\phi_{622}(t)/dt=\Delta V_1[\langle R_0\rangle(t)]-\omega_0$ (green graphs) and $\Delta V_1[\langle R_1\rangle(t)]-\omega_0$ (blue graphs); the 811 nm field has $d\phi_{811}(t)/dt=\Delta V_1[\langle R_0\rangle(t)]-\omega_0$ to optimize $|1\rangle\leftarrow|0\rangle$ absorption in all cases. The main body of each diagram shows $p_{n_{X(3)}}(t=2\sigma)$ for all vibrational levels with values shown by the scale of the right-hand ordinate; the inset to each diagram magnifies $p_{X(3)}(t=2\sigma)$ for $n_{X(3)}=0-40$ with values indicated by scale of the left-hand ordinate. Graphs labeled "*r*," "*g*," and "*b*" designate red, green, and blue, respectively.

(6) to optimize $|1\rangle\leftarrow|0\rangle$ absorption with those obtaining to transform-limited fields. Normalized probabilities of electron energy-resolved ionization by one- and two-color fields at the end of 1 ps pulses are displayed in Fig. 8, where we distinguish between the probabilities $p^{(r)}_{2\leftarrow0}(\varepsilon_\mathbf{k};t=2\sigma)$ and $p^{(r)}_{2\leftarrow1\leftarrow0}(\varepsilon_\mathbf{k};t=2\sigma)$ of nonresonant and resonant ionization via $|1\rangle$ of order $r=2$ or 3. Because values of $p^{(3)}_{2(\leftarrow1)\leftarrow0}(\varepsilon_\mathbf{k};t=2\sigma)$ and $p^{(2)}_{2(\leftarrow1)\leftarrow0}(\varepsilon_\mathbf{k};t=2\sigma)$ differ by 10^{14} over the energy range $\varepsilon_\mathbf{k}=0-1779$ meV, the spectra are presented as semilogarithmic plots of the ionization probability. The general features of the spectra concern their structure and relative magnitudes under different driving field conditions. Both $p^{(3)}_{2\leftarrow1\leftarrow0}(\varepsilon_\mathbf{k};t=2\sigma)$ (red spectra) and $p^{(3)}_{2\leftarrow0}(\varepsilon_\mathbf{k};t=2\sigma)$ (blue spectra) resulting from three-photon ionization by a transform-limited 811 nm pulse [Figs. 8(a) and 8(b)] exhibit maxima at $\varepsilon_\mathbf{k}\simeq880$ meV, whereas the probability of two-photon ionization at $\lambda=622$ nm increases in line with the $\sqrt{\varepsilon_\mathbf{k}}$ dependence of the transition dipole moment [Fig. 8(c)]. The relative sensitivity of ionization probability to electron kinetic energy in the former case can be explained

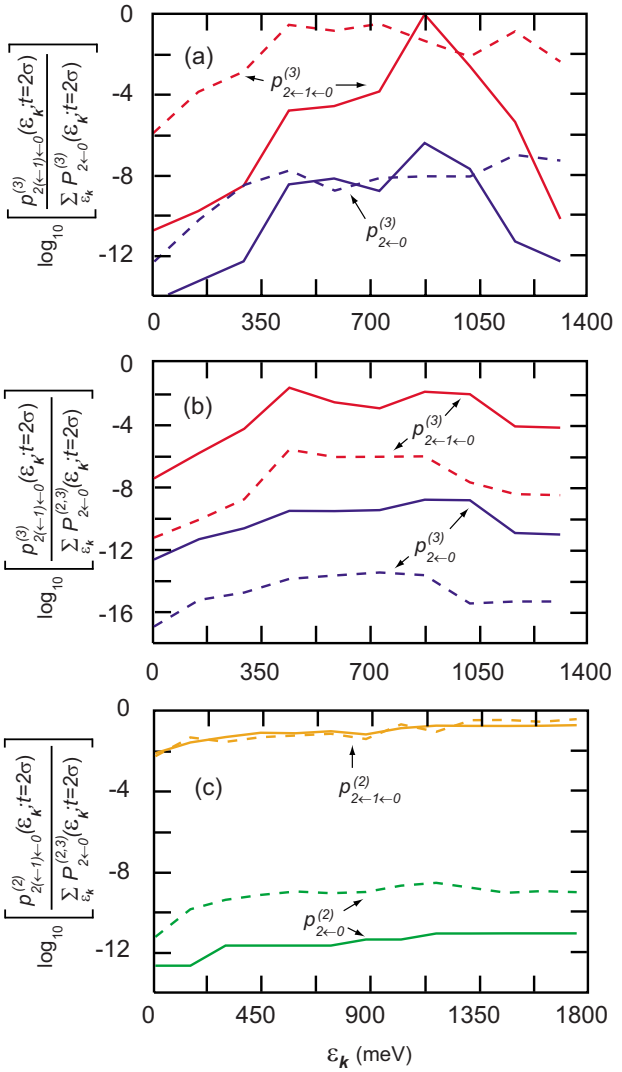

FIG. 8. (Color online) Semilogarithmic plots of electron energy spectra of three-photon [(a) and (b)] and two-photon [(c)] ionization of Rb+Cs at the end ($t=2$ ps) due to a 1 ps chirped field with maximum field strength $|\mathbf{E}_0|=2.5\times10^{-4}$ a.u. Graph (a) shows $p^{(3)}_{2\leftarrow0}(\varepsilon_\mathbf{k};t=2\sigma)$ (blue spectra) and $p^{(3)}_{2\leftarrow1\leftarrow0}(\varepsilon_\mathbf{k};t=2\sigma)$ (red spectra) for direct and resonance-enhanced ionization driven by a single-color field at $\lambda_0=811$ nm. Graph (b) shows the same probabilities for ionization by the 811 nm component of a bichromatic field and graph (c) shows $p^{(2)}_{2\leftarrow0}(\varepsilon_\mathbf{k};t=2\sigma)$ (green spectra) and $p^{(2)}_{2\leftarrow1\leftarrow0}(\varepsilon_\mathbf{k};t=2\sigma)$ (orange spectra) driven by the 622 nm component. The filled (dashed) spectra in (a) show the probabilities for driving fields with $d\phi_{811}(t)/dt=0$ ($\Delta V_1[\langle R_0\rangle(t)]-\omega_0$). In (b) and (c), the filled (dashed) spectra show probabilities when $d\phi_{622}(t)/dt=0$ ($\Delta V_1[\langle R_0\rangle(t)]-\omega_0$) and $d\phi_{811}(t)/dt=\Delta V_1[\langle R_0\rangle(t)]-\omega_0$. A transition moment $\mathbf{d}_{2\leftarrow0}$ given by Eq. (A1) with $d=2$ is used in all calculations. The spectra are normalized with respect to the total ionization probability at $t=2\sigma$, i.e., with respect to $\Sigma_{\varepsilon_\mathbf{k}}P^{(3)}_{2\leftarrow0}(\varepsilon_\mathbf{k};t=2\sigma)=1$ in (a) and to $\Sigma_{\varepsilon_\mathbf{k}}P^{(2,3)}_{2\leftarrow0}(\varepsilon_\mathbf{k};t=2\sigma)=1$ in (b) and (c), where $P^{(2,3)}_{2\leftarrow0}(\varepsilon_\mathbf{k};t=2\sigma)$ signifies $P^{(3)}_{2\leftarrow0}(\varepsilon_\mathbf{k};t=2\sigma)+P^{(2)}_{2\leftarrow0}(\varepsilon_\mathbf{k};t=2\sigma)+$interference terms.

as a reflection of resonance between $V_1(R)-V_0(R)$ and the photon energy over a relatively small range of atomic separations intermediate between separated atoms (which would favor Cs atom ionization at $\varepsilon_\mathbf{k}=694$ meV) and bound quan-

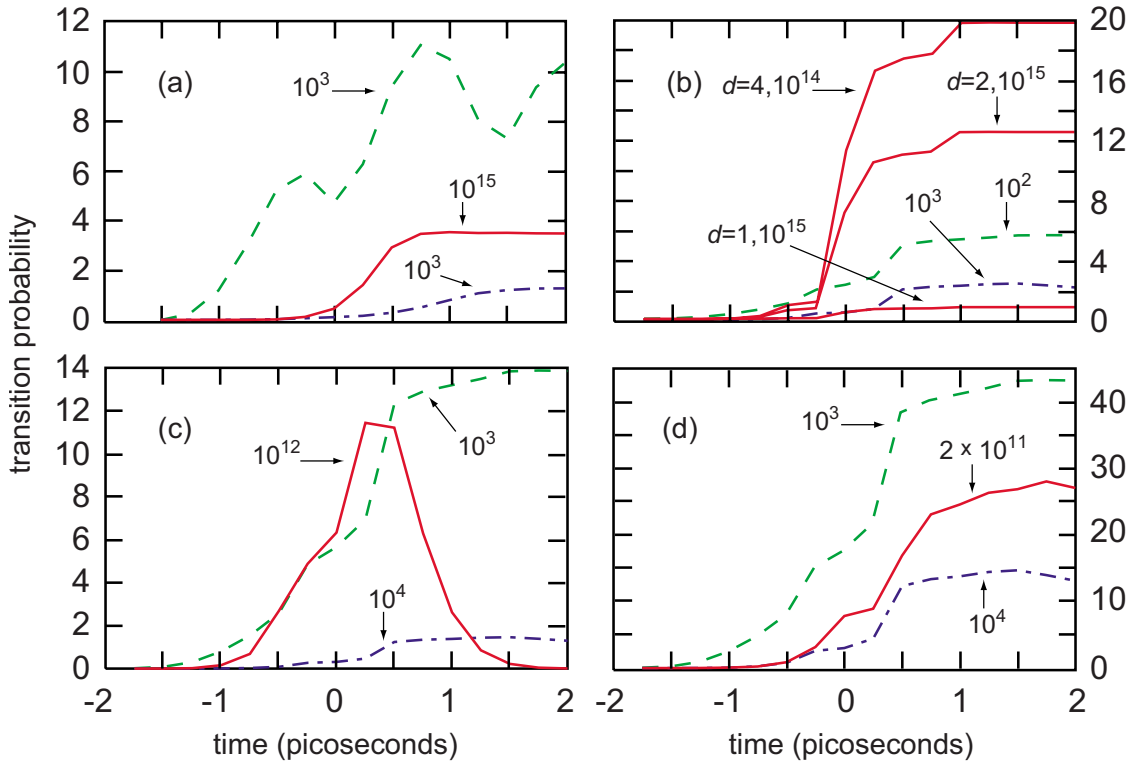

FIG. 9. (Color online) Comparison of total ionization probabilities (red curves) of Rb+Cs with the neutral bound-state probabilities $\|\psi_1^{(1)}(R \leqslant 10\ \text{Å};t)\|^2$ (green dashed curves) and $\|\psi_0^{(2)}(R \leqslant 10\ \text{Å};t)\|^2$ (blue dotted-dashed curves). Graphs (a) and (b) pertain to photoassociation by a single-color pulse at λ_0=811 nm with $d\phi(t)/dt=0$ and $\Delta V_1[\langle R_0\rangle(t)]-\omega_0$, respectively, and the ionization probability is $P^{(3)}_{2\leftarrow 0}(t)$. Graphs (c) and (d) pertain to photoassociation by a bichromatic field at λ_0=811 and 622 nm in which $d\phi_{622}(t)/dt=0$ and $\Delta V_1[\langle R_0\rangle(t)]-\omega_0$, respectively, $d\phi_{811}(t)/dt=\Delta V_1[\langle R_0\rangle(t)]-\omega_0$ and the ionization probability is $P^{(2,3)}_{2\leftarrow 0}(t)$. The duration of both single- and two-color pulses is σ=1 ps and the maximum field strength is $|\mathbf{E}_0|=2.5\times 10^{-4}$ a.u. Graph (b) shows $P^{(3)}_{2\leftarrow 0}(t)$ for different magnitudes of the transition dipole for ionization given by Eq. (A1) with d=1, 2, and 4. All probabilities are normalized with respect to $|U^{(0)}(t,t_0)|^2=1$ at $t=2\sigma$ with $t_0=-2\sigma$. The powers of ten indicate the multiplication factors applied to the divers probabilities.

tum levels supported by $3^1\Sigma^+$ potential (which would favor ionization to $1^2\Sigma^+$ $RbCs^+$ at $\varepsilon_{\mathbf{k}}>694$ meV). Inspection of the abscissas of Figs. 8(a)–8(c) reveals the extent to which resonance-enhanced electron removal dominates direct ionization at either wavelength: at λ=811 (622) nm the difference in probability is on the order 10^4–10^6 (10^8–10^{11}) at different electron energies. The predominance of the resonant channel is maintained at all times during the pulse, and at all electron kinetic energies, in addition to the results shown here for $t=2\sigma=2$ ps. A consequence of the disparity between $p^{(r)}_{2\leftarrow 1\leftarrow 0}(\varepsilon_{\mathbf{k}};t)$ and $p^{(r)}_{2\leftarrow 0}(\varepsilon_{\mathbf{k}};t)$ is that interference between the two pathways leading to electrons at a given $\varepsilon_{\mathbf{k}}$ is swamped by the preponderance of resonant ionization.

Figure 9 compares the probability of ionization (at all $\varepsilon_{\mathbf{k}}$) with the occupation probabilities of the neutral excited state due to photon absorption and the ground state due to absorption and stimulated reemission. When a transform-limited field at 811 nm is applied to the Rb+Cs collision at a field strength $|\mathbf{E}_0|=2.5\times 10^{-4}$ a.u., the probability of ionization is on the order of 10^{12} times lower than that for generation of neutral ground-state molecules by photon absorption and stimulated reemission, and increases by a factor of 2 when the phase of the field is modulated to optimize $|1\rangle\leftarrow|0\rangle$ absorption. The effect of adjusting the magnitude of the transition moment for ionization via the parameter d in Eq. (A1) is examined in Fig. 9(b), from which it is found that increasing $|\mathbf{d}_{2\leftarrow 0}|$ by a factor of 4 enhances the asymptotic ionization level by a factor of about 250. The ionization probability increases by a factor of approximately 1000 when a bichromatic field with components at 622 and 811 nm at the same total field strength is applied to the collision, as shown in Figs. 9(c) and 9(d), and so always remains smaller than the probabilities of transitions between neutral electronic states.

The ratio of the cumulative ionization probabilities $\int_{-2\sigma}^{2\sigma} P^{(3)}_{2\leftarrow 0}(t)dt$ and $\int_{-2\sigma}^{2\sigma} P^{(2,3)}_{2\leftarrow 0}(t)dt$ relative to the probability $P^{(2)}_{0\leftarrow 0}(t=2\sigma)$ of a pump-dump transition at $t=2\sigma$ represents a measure, valid within the Born-Oppenheimer approximation (as well as the other simplifications invoked in these calculations), of the minimum probability with which stimulated emission to specific vibrational levels of the $X^1\Sigma^+$ state must occur, if they are to remain populated at times after application of the photoassociation field to an extent which enables their subsequent detection (by narrowband laser light, for example). For a single-color field at λ_0=811 nm with $|\mathbf{E}_0|=2.5\times 10^{-4}$ a.u. we find $\int_{-2\sigma}^{2\sigma} P^{(3)}_{2\leftarrow 0}(t)dt/P^{(2)}_{0\leftarrow 0}(t=2\sigma)=2.3\times 10^{-11}$ when the temporal phase of the field is constant and 0.3 (0.9), 4.4 (14), and 70(220)$\times 10^{-11}$ when the phase of the driving field is modulated by $\Delta V_1[\langle R_0\rangle(t)]$ ($\Delta V_2[\langle R_0\rangle(t)]$) to optimize $|1\rangle\leftarrow|0\rangle$ absorption and the transition dipole moment for ionization is given by Eq. (A1) with d=1, 2, and 4,

respectively. Comparison of these ratios with the vibrational probabilities used to construct Fig. 5 indicates that state-resolved pump-dump transitions to all vibrational levels of the $X^1\Sigma^+$ state are more probable than three-photon ionization irrespective of the modulation applied to the temporal phase of the driving field and of the three values of d.

When a bichromatic field at $|\mathbf{E}_0|=2.5\times10^{-4}$ a.u. drives photoassociation, we find $\int_{-2\sigma}^{2\sigma}P_{2\leftarrow0}^{(2,3)}(t)dt/P_{0\leftarrow0}^{(2)}(t=2\sigma)=2.9,5.8$, and 21.5×10^{-7} when $d=2$ and the phase of the shorter-wavelength component is zero and modulated by $\Delta V_1[\langle R_0\rangle(t)]$ and $\Delta V_2[\langle R_0\rangle(t)]$, respectively. When the shorter-wavelength field is transform limited, pump-dump transitions to n_X levels remain more probable than two- and three-photon ionization for all destination levels except for $n_X=0$, 134, and 135 located at the extremities of the $X^1\Sigma^+$ potential well. When the temporal phase of the 622 nm field is chirped, transitions to between 4 and 21 bound levels with $0\leqslant n_X\leqslant43$ become less probable than ionization due to their unfavorable overlap with wave function amplitude in the $3^1\Sigma^+$ state. Stimulated emission to higher lying oscillator levels of the $X^1\Sigma^+$ potential remains, however, more probable than ionization loss so that detection of molecules in these levels may therefore be profitably carried out after the photoassociating fields have exited the target volume.

The probabilities given in the preceding paragraph retain their validity only to the extent as do the dipole moments adopted in this work for the neutral absorption and ionization transitions of interest (see the Appendix, Sec. II). Nevertheless, the qualitative conclusion that can be drawn from the comparison given above is that state-resolved detection of individual vibrational levels would appear in principle feasible for all oscillator levels of the $X^1\Sigma^+$ state when photoassociation is guided by a field centered at $\lambda_0=811$ nm operating under weak-field conditions. The substantially higher probability of ionization incurred when the photoassociation is driven by a bichromatic field may counteract the apparent advantage of stimulating emission to deeply bound vibrational levels of the molecular electronic ground state. The numerical simulations demonstrate that modulating the phase of the shorter-wavelength component in terms of $\Delta V_2[R(t)]$ reduces further the potential for vibrational state-resolved detection of $X^1\Sigma^+$ molecules compared to that obtaining when $\phi_{622}(t)$ is modulated by $\Delta V_1[R(t)]$.

If a probe of the dynamics of molecule formation during photoassociation is sought, values of $p_{2\leftarrow1\leftarrow0}^{(2)}(\varepsilon_\mathbf{k};t)$ and $p_{2\leftarrow1\leftarrow0}^{(3)}(\varepsilon_\mathbf{k};t)$ relative to $P_{0\leftarrow0}^{(2)}(t)$ suggest that this could be affected by an additional ionizing field whose wavelength is selected so as to generate ions at energies $\varepsilon_\mathbf{k}$ removed from peaks in the electron energy spectra (Fig. 8) due to resonance-enhanced ionization. A consequence of the slow translatory motion of $\psi_0^{(2)}(R;t)$ and $\psi_1^{(1)}(R;t)$ relative to their spreading is, however, that a time-resolved measurement, in which a second femtosecond pulse is applied to the colliding atoms at different times relative to the photoassociation pulse, would exhibit only weakly modulated bursts of ionization due to the wave-packet evolution. The effect is exacerbated by the extended (4 ps) period of photon absorptions and stimulated emissions. The modulation depth depends also on the initial width of the zeroth-order wave packet, but we have not systematically investigated this effect. The effects of the slow wave packet motion contrast with the nearly fully modulated ion signal characteristic of the vibrational motion of a strongly localized wave packet generated when photoabsorption imparts a large relative kinetic energy to the oscillating nuclei of a molecule [26].

IV. CONCLUSIONS

This work considers photoassociation of $5s_{1/2}$ ^{85}Rb $+6s_{1/2}$ ^{133}Cs atoms at $T=2$ mK to generate bound levels of the $(1)0^+\leftrightarrow X^1\Sigma^+$ molecular ground state by successive stimulated absorption and emission to and from the $(4)0^+\leftrightarrow3^1\Sigma^+$ state. At this temperature, the collision takes about 3 ps to complete one oscillation at $R\leqslant10$ Å. The principal effects of the application of a broadband optical field with a maximum amplitude $|\mathbf{E}_0|=2.5\times10^{-4}$ a.u. centered at 811 nm and different temporal phases, as evidenced by this theoretical study, are as follows:

(i) Photoassociation leading to the $X^1\Sigma^+$ molecular ground state without regard to the destination oscillator level is optimally achieved by a driving field whose temporal phase maximizes the probability of $(4)0^+\leftarrow(1)0^+$ photon absorption rather than stimulated emission. Generation of maximum amplitude in the $X^1\Sigma^+$ state is optimally achieved by a 1 ps field with a time-dependent frequency $\omega(t)$ which varies in accord with the classical potential energy difference between the $(1)0^+$ and $(4)0^+$ atom-atom interactions at all interatomic separations, and by a 355 fs field down chirped so that $\omega(t)$ matches the linearized energy difference between the attractive limbs of the potential curves sampled by outwards-bound wave packets.

(ii) A driving field whose temporal phase matches $\omega(t)$ to the shape of the ground-state potential (referred to the potential energy at the location of the initially excited wave packet) results in dissociation of incipient molecules to separate $5p_{1/2}$ Rb$+6s_{1/2}$ Cs atoms in addition to photoassociation. As a consequence, the action of fields phase modulated in this way is to suppress generation of molecules relative to the probability of photoassociation by transform-limited pulses and their formation at thermal equilibrium in the absence of light. Linearly up-chirped Gaussian driving fields have the same effect. Driving fields which are phase-modulated by the classical difference potential or which are linearly down chirped enhance the generation of bound quantum states compared to bandwidth-limited fields and the thermal probability.

(iii) A transform-limited driving field centered at 811 nm stimulates transitions to a narrow band of high-lying vibrational levels of the $3^1\Sigma^+$ excited state centered around $n_3=118$. In contrast, phase-modulated fields deposit population across a range of vibrational levels $n_3\simeq50-65$ which are bound by approximately half the well depth; subsequent stimulated emission transitions to more deeply bound oscillator levels of the $X^1\Sigma^+$ state result from application of such fields. Maximal population in vibrational levels of the $X^1\Sigma^+$ state generated by pump-dump transitions is clustered around high-lying levels in the range $90\leqslant n_X\leqslant120$ when the temporal phase of the driving field is modulated or constant. At $|\mathbf{E}_0|=2.5\times10^{-4}$ a.u., the relative probabilities of individual

vibrational levels of the $3^1\Sigma^+$ state and $X^1\Sigma^+$ states [normalized so that $\Sigma_{n_{X(3)}} p_{n_{X(3)}}(t=2\sigma)=1$] vary between 4.3×10^{-11} and 0.43 and between 7.6×10^{-9} and 0.29, respectively, at the end of a transform-limited 1 ps pulse.

(iv) Transitions to deeply bound oscillator levels of the $X^1\Sigma^+$ electronic state are optimally effected by 811 nm fields whose temporal phase is chirped to enhance $(4)0^+\rightarrow(1)0^+$ stimulated emission rather than absorption, in contrast to the situation in respect to formation of $X^1\Sigma^+$ RbCs without regard to vibrational specificity. The relative occupation probabilities of levels $n_X\leqslant10$ at the end of a 1 ps driving field chirped to promote stimulated emission range from 6.2×10^{-8} to 2.0×10^{-4} (subject to the normalization criterion given in the previous paragraph). Taking into account the amplitudes of transitions between the electronic states, the probabilities relative to the starting collision pair are 1×10^{-10} and 8×10^{-10} for $n_X=0$ when $\phi(t)$ is modulated by the classical difference potential and the shape of the ground-state potential, respectively; for other levels with $n_X\leqslant10$, probabilities on the order of 10^{-7} are achieved. Under weak-field light-atom interaction conditions, the variation in occupation probability is influenced, but not exclusively determined, by the Franck-Condon overlap between vibrational eigenfunctions of the optically connected states.

To investigate the possibility of enhancing photoassociation to oscillator levels of the $X^1\Sigma^+$ state with $n_X\leqslant10$, the action of a broadband field with components of equal amplitude $|\mathbf{E}_0|=1.25\times10^{-4}$ a.u. centered at 811 and 622 nm was studied. To include ionization of the colliding atoms, a model transition dipole moment based on that for the $(4)0^+\leftrightarrow(1)0^+$ transition between neutral states was invoked. The principal findings of these calculations were as follows:

Generation of vibrational levels $n_x\leqslant10$ of the $X^1\Sigma^+$ state becomes more favorable, typically by a factor on the order of 10, compared to the probabilities excited by the single-color field; the exception to the enhancement is the zero-point level, whose amplitude remains about the same at the end of photoassociation driven by single-color and bichromatic 1 ps fields. The increase in probability of generating deeply bound oscillator levels is offset by an increased probability of two-photon ionization which renders several (but not all) low-lying levels of the $X^1\Sigma^+$-state molecule inaccessible at the end of the bichromatic driving field; mid- and high-lying levels with $n_X\geqslant44$ remain intact, however.

Under weak-field conditions stipulated by $|\mathbf{E}_0|=2.5\times10^{-4}$ a.u. and for the form of the transition dipole moment for ionization adopted in this work [Eq. (A1)], the probability of three-photon ionization at a given time during a 811 nm pulse is on the order of $0.1-30\times10^{11}$ lower than that for pump-dump transitions to the neutral electronic ground state, depending on the temporal phase. When driven by a bichromatic field of the same amplitude, the total ionization probability is due overwhelmingly to resonance-enhanced two-photon transitions via the $(4)0^+$ state. Compared to single-color ionization by a field phase-modulated to maximize $(4)0^+\leftarrow(1)0^+$ absorption, the probabilities of ionization prompted by the biochromatic field is a higher by a factor of between approximately 3000 and 10^4 for different temporal phases applied to the shorter-wavelength field. Given the dipole moment function adopted for the ionization transitions, the calculations reported here suggest that the combination of two- and three-photon ionization at 622 and 811 nm is sufficiently probable at an overall field strength of $|\mathbf{E}_0|=2.5\times10^{-4}$ a.u. to mask pump-dump transitions to specific oscillator levels near the minimum of the $X^1\Sigma^+$ state.

In summary, it would seem on the basis of these calculations that phase-modulated fields operating over a picosecond time scale under weak-field conditions could be favorably applied to generate cold molecules in specific vibrational levels in the mid- to upper reaches of the $X^1\Sigma^+$ potential well. Further, it would seem that generation of deeply bound nuclear quantum states near the minimum of the ground electronic state may be profitably pursued with driving fields chosen such that at least three photons are required for ionization; this requirement ensures that the probability of ionization remains sufficiently small to allow subsequent detection of neutral molecules with vibrational state resolution.

ACKNOWLEDGMENTS

This work was supported by E.P.S.R.C. through Grant No. EP/D003555/1 and A.H. thanks E.P.S.R.C. for financial assistance. We acknowledge helpful discussions with C.S. Adams, S. Cornish, I.G. Hughes, and I. Mourachko of Durham University.

APPENDIX

This appendix supplies basic information required for calculation of the probability amplitudes given by Eqs. (1)–(3).

1. Hamiltonian operators

The field-free Hamiltonians for collision of the two atoms in neutral and ionic states are

$$H_q = |q\rangle[-\nabla^2/2 + V_q(R)]\langle q|$$

and

$$H_q = \int_0^{\varepsilon_{\mathbf{k}_{\max}}} |q;\varepsilon_{\mathbf{k}}\rangle[-\nabla^2/2 + V_q(R) + \varepsilon_{\mathbf{k}}]\langle q;\varepsilon_{\mathbf{k}}|\mathrm{d}\varepsilon_{\mathbf{k}},$$

respectively, where $-\nabla^2/2$ is the nuclear kinetic energy operator, $|q\rangle$ designates eigenstates of the neutral atomic pair and $|q;\varepsilon_{\mathbf{k}}\rangle$ eigenstates of the atom+ion combination; the latter are explicitly labeled by the kinetic energy $\varepsilon_{\mathbf{k}}$ of the free electron, but also contain the state of the core electrons of the Rb+Cs atoms. For the diabatic potential curves $V_q(R)$ adopted in this work, three-photon ionization at $\lambda_0=811\pm27$ nm generates electrons with a maximum kinetic energy $\varepsilon_{\mathbf{k}_{\max}}=1314\pm52$ meV at molecular configurations (above the minimum of the $X^2\Sigma^+$ $RbCs^+$ potential), reducing to $\varepsilon_{\mathbf{k}}=694\pm52$ meV at the atomic asymptote ($R\rightarrow\infty$). Likewise, two-photon ionization at $\lambda_0=622\pm16$ nm generates electrons with energies between $\varepsilon_{\mathbf{k}}=94\pm52$ and 714 ± 52 meV, while the combination of two 811 nm photons coupled with a single photon at 622 nm ionizes the atomic pair with electron energies between 1158 ± 58 and 1779 ± 58 meV.

The diabatic potentials curves shown in Fig. 1(a) for the $(1)0^+$ and $(4)0^+$ states of the neutral molecule and the $(1')0^+$ ground state of the ion were constructed from a cubic spline fit to the data points provided by Allouche and co-workers from relativistic *ab initio* calculations [18]. Dynamic Stark shifts of the electronic states were omitted from the H_q by restricting the strength of the light-atom (-molecule) interaction to within the weak-field regime as detailed in Sec. II B. The Hamiltonian for the molecular ion was established on a discretized grid of equally spaced electron kinetic energies. Because the amplitudes for ionization via both direct (nonresonant) and resonant channels were maximal at particular energies (see Sec. III D), a grid comprising twelve values of $\varepsilon_{\mathbf{k}}$ equally spaced by 162 meV between zero and 1779 meV was found to be sufficient to characterize the main features of the electron energy spectra. These spectra were qualitatively the same as those deriving from calculations of H_q which adopted an energy spacing of 50 meV equal to the photon energy resolution of a transform-limited field centered at 811 nm.

2. Transition dipole moments

The transition dipole moment which connects the $|1\rangle$ and $|0\rangle$ states does not appear to have been calculated from studies of the electronic structure of RbCs. Of more relevance to calculations of $A^{(1)}_{1\leftarrow 0}(t)$ and $A^{(2)}_{0\leftarrow 0}(t)$ reported in this work is a realistic attempt to take into account the distance variation of the transition dipole rather than an estimate of its absolute magnitude, so long as the light-atom interaction is maintained within the weak-field regime. Accordingly, $|\mathbf{d}_{1\leftrightarrow 0}|$ for the $|1\rangle\leftrightarrow|0\rangle$ transition was constructed from the dipole moments for the $(3)0^+\leftrightarrow(1)0^+$ and $(2)0^+\leftrightarrow(1)0^+$ transitions provided in Ref. [23] of [20] from relativistic *ab initio* calculations of the low-lying states which correlate with $6p_{1/2,3/2}$ Cs+$5s_{1/2}$ Rb: the dipole moment for $(3)0^+\leftrightarrow(1)0^+$ (corresponding to the $2^1\Sigma^+\leftrightarrow X^1\Sigma^+$ transition between molecular states) was used for $R\leqslant 10$ a.u. and that for $(2)0^+\leftrightarrow(1)0^+$ (which contributes to the $6p_{1/2}\leftrightarrow 6s_{1/2}$ atomic Cs transition) for $R>10$ a.u. The result is a dipole moment function which reaches a maximum of $|\mathbf{d}_{1\leftarrow 0}|=5.037$ a.u. at $R=12.5$ a.u. [see Fig. 6(a) of Ref. [20]]. There appears likewise to be no information on dipole moments for ionization of Rb+Cs states. To compare the probability of ionization with that for the $(4)0^+\leftarrow(1)0^+$ transition between neutral states, $|\mathbf{d}_{2\leftarrow 0}|$ (in a.u.) was represented by

$$|\mathbf{d}_{2\leftarrow 0}| = d(0.5396 + 1.7575\sqrt{\varepsilon_{\mathbf{k}}/[\mathrm{eV}]}) \qquad \text{(A1)}$$

to take account of the variation in the density of electron continuum states accessible at different $\varepsilon_{\mathbf{k}}$. Integer values $d=1$, 2, and 4 give maximum values of $|\mathbf{d}_{2\leftarrow 0}|$ at $\varepsilon_{\mathbf{k}}=1314$ meV which are approximately two times smaller, the same, and two times larger than the maximum dipole moment for the neutral absorption transition.

3. Numerical evaluation of Eqs. (6) and (7)

To evaluate the integrals of Eqs. (6) and (7), a discretized time interval was chosen such that it satisfied the condition

$$\Delta t \ll \left| \frac{1}{\mathbf{v}(t)} \frac{\Delta V_n[R(t)]}{\nabla V_q[R(t)]} \right| \qquad \text{(A2)}$$

for all times during the oscillation of the wave packet in the starting state $|q\rangle$, where the potential gradient is $\nabla V_q[R(t)]$ along the interatomic coordinate and the wave-packet velocity is $\mathbf{v}(t)$ at the midpoint of Δt: $n=1$ or 2 in Eq. (A2) and $q=0$ or 1 for optimization of $|1\rangle\leftrightarrow|0\rangle$ absorption or stimulated emission, respectively. Application of condition (A2) with the replacement $\Delta V_n[R(t)]\rightarrow\Delta V_n[\langle R_q\rangle(t)]$ (see Sec. II B) requires that the nuclear wave-packet motion in the qth electronic state adhere to Ehrenfest's theorem throughout the pulse duration, i.e., that $\langle\nabla V_q[R(t)]\rangle=\nabla V_q[\langle R_q\rangle(t)]$ at all t. In practice, the numerical accuracy of the evaluations of Eqs. (6) and (7) was checked by repeatedly halving the time interval at which $\Delta V_n[\langle R_q\rangle(t)]$ was evaluated within a given total propagation time until the norms of the wave packets on the optically connected states varied by less than 10^{-3}, irrespective of the width of the starting wave function relative to $|\Delta V_n[\langle R_q\rangle(t)]/\nabla V_q[\langle R_q\rangle(t)]|$: a typical value for Δt was 250 fs for a total wave-packet propagation time of 4 ps.

4. Numerical information

Nuclear wave-functions were advanced in time using the split-operator method [27] over discretized potential energy curves ranging from 2.7 to 120.0 Å with 8192 or 16384 grid points chosen to ensure convergence of the wave-packet motion in coordinate and momentum space in all electronic states. A complex absorbing potential (CAP) of the type described in Ref. [28] was invoked to suppress wave-function amplitude at $R\geqslant 116$ Å, but to avoid the unwieldliness of setting up different CAPs for wave functions with large and differing relative spreads in kinetic energy at the three atomic asymptotes, most calculations made use of long grid formations without any absorbing capability. Small amplitudes of $\psi^{(3)}_2(R;t;\varepsilon_{\mathbf{k}})$ corresponding to separated $5p_{1/2}$ Rb+$5p^6_0$ Cs^+ reached distances $R\geqslant 110$ Å after 4 ps of propagation during the broadest laser fields investigated here. Numerically stable wave packets in the neutral and ion states were advanced with discretizations of $\leqslant 0.4$ fs in all propagations.

[1] B. Chatel and B. Girard, in *Femtosecond laser spectroscopy*, edited by P. Hannaford (Springer, New York, 2005), Ch. 10, pp. 267–304; J. Phys. B **41**, 070201 (2008), special issue on coherent control, edited by H. Fielding, M. Shapiro and T. Baumert.

[2] Eur. Phys. J. D **31**, 149 (2004), special issue on cold polar molecules, edited by J. Doyle, B. Friedrich, R. V. Krems, and F. Masnou-Seeuws; J. Phys. B **39**, S813 (2006), special issue on cold molecules, edited by O. Dulieu, M. Raoult, and E. Tiemann.

[3] E. R. Hudson, H. J. Lewandowski, B. C. Sawyer, and J. Ye, Phys. Rev. Lett. **96**, 143004 (2006); C. Chin and V. V. Flambaum, *ibid.* **96**, 230801 (2006); T. Zelevinsky, S. Kotochigova, and J. Ye, *ibid.* **100**, 043201 (2008); D. DeMille, S. Sainis, J. Sage, T. Bergeman, S. Kotochigova, and E. Tiesinga, *ibid.* **100**, 043202 (2008).

[4] J. J. Hudson, B. E. Sauer, M. R. Tarbutt, and E. A. Hinds, Phys. Rev. Lett. **89**, 023003 (2002).

[5] K. V. Kheruntsyan, M. K. Olsen, and P. D. Drummond, Phys. Rev. Lett. **95**, 150405 (2005); K. V. Kheruntsyan, *ibid.* **96**, 110401 (2006); P. Milman, A. Keller, E. Charron, and O. Atabek, *ibid.* **99**, 130405 (2007); C. M. Savage and K. V. Kheruntsyan, *ibid.* **99**, 220404 (2007).

[6] A. Micheli, G. K. Brennen, and P. Zoller, Nat. Phys. **2**, 341 (2006); P. Rabl, D. DeMille, J. M. Doyle, M. D. Lukin, R. J. Schoelkopf, and P. Zoller, Phys. Rev. Lett. **97**, 033003 (2006).

[7] G. Pupillo, A. Griessner, A. Micheli, M. Ortner, D.-W. Wang, and P. Zoller, Phys. Rev. Lett. **100**, 050402 (2008); N. Syassen *et al.*, Science **320**, 1329 (2008).

[8] (a) J. Vala, O. Dulieu, F. Masnou-Seeuws, P. Pillet, and R. Kosloff, Phys. Rev. A **63**, 013412 (2000); (b) M. Vatasescu, O. Dulieu, R. Kosloff, and F. Masnou-Seeuws, *ibid.* **63**, 033407 (2001); (c) E. Luc-Koenig, R. Kosloff, F. Masnou-Seeuws, and M. Vatasescu, *ibid.* **70**, 033414 (2004); (d) C. P. Koch, R. Kosloff, E. Luc-Koenig, F. Masnou-Seeuws, and A. Crubellier, J. Phys. B **39**, S1017 (2006); (e) S. Kallush and R. Kosloff, Phys. Rev. A **77**, 023421 (2008).

[9] (a) E. Luc-Koenig, M. Vatasescu, and F. Masnou-Seeuws, Eur. Phys. J. D **31**, 239 (2004); (b) U. Poschinger *et al.*, J. Phys. B **39**, S1001 (2006).

[10] (a) C. P. Koch, E. Luc-Koenig, and F. Masnou-Seeuws, Phys. Rev. A **73**, 033408 (2006); (b) C. P. Koch, R. Kosloff, and F. Masnou-Seeuws, *ibid.* **73**, 043409 (2006); (c) B. L. Brown and I. A. Walmsley, J. Phys. B **39**, S1055 (2006); (d) J. Mur-Petit, E. Luc-Koenig, and F. Masnou-Seeuws, Phys. Rev. A **75**, 061404(R) (2007).

[11] E. A. Shapiro, M. Shapiro, A. Pe'er, and J. Ye, Phys. Rev. A **75**, 013405 (2007); A. Pe'er, E. A. Shapiro, M. C. Stowe, M. Shapiro, and J. Ye, Phys. Rev. Lett. **98**, 113004 (2007); E. A. Shapiro, V. Milner, C. Menzel-Jones, and M. Shapiro, *ibid.* **99**, 033002 (2007).

[12] J. G. Danzl *et al.*, Science **321**, 1062 (2008).

[13] (a) M. J. Wright, S. D. Gensemer, J. Vala, R. Kosloff, and P. L. Gould, Phys. Rev. Lett. **95**, 063001 (2005); (b) M. J. Wright, J. A. Pechkis, J. L. Carini, and P. L. Gould, Phys. Rev. A **74**, 063402 (2006); (c) M. J. Wright, J. A. Pechkis, J. L. Carini, S. Kallush, R. Kosloff, and P. L. Gould, *ibid.* **75**, 051401 (2007).

[14] (a) B. L. Brown, A. J. Dicks, and I. A. Walmsley, Phys. Rev. Lett. **96**, 173002 (2006); (b) W. Salzmann *et al.*, Phys. Rev. A **73**, 023414 (2006); (c) F. Weise *et al.*, *ibid.* **76**, 063404 (2007); (d) W. Salzmann *et al.*, Phys. Rev. Lett. **100**, 233003 (2008); (e) M. Viteau *et al.*, Science **321**, 232 (2008).

[15] Information on the spectroscopy and potential energy curves for Cs+Cs and Rb+Rb can be found, respectively, in Refs. [9(a),9(b)] and references therein.

[16] The center wavelength and bandwidth of the applied field were chosen to match that stated by a commercial vendor of amplified Ti:sapphire lasers.

[17] A. J. Kerman, J. M. Sage, S. Sainis, T. Bergeman, and D. DeMille, Phys. Rev. Lett. **92**, 153001 (2004); J. M. Sage, S. Sainis, T. Bergeman, and D. DeMille, *ibid.* **94**, 203001 (2005).

[18] (a) M. Korek and A. R. Allouche, J. Phys. B **34**, 3689 (2001); (b) H. Fahs, A. R. Allouche, M. Korek, and M. Aubert-Frécon, *ibid.* **35**, 1501 (2002).

[19] Relativistic *ab initio* calculations of RbCs by Kotochigova and Tiesinga [20] reveal curve crossings between diabatic states which correlate with the $5s_{1/2}$ Rb+$6p_{1/2,3/2}$ Cs asymptote at R_x=7.14 and 5.29 Å. Electronic states at interatomic separations $R<R_x$ are appropriately labeled in nonrelativistic Hund's case (a) notation, while Hund's case (c) labeling pertains at separations $R>R_x$. The potential curve calculated by Allouche and co-workers [18] for the $(4)0^+$ state which correlates with $5p_{1/2}$ Rb+$6s_{1/2}$ Cs, exhibits no avoided crossing at $R>6.0$ a.u. with the $(5)0^+$ potential leading to $5p_{3/2}$ Rb+$6s_{1/2}$ Cs.

[20] S. Kotochigova and E. Tiesinga, J. Chem. Phys. **123**, 174304 (2005).

[21] R. J. Le Roy, LEVEL 8.0: University of Waterloo Chemical Physics Research Report No. CP-663 (2007), see http://leroy.uwaterloo.ca/programs/.

[22] To avoid notational problems associated with a change of angular momentum coupling, we refer to the neutral ground and excited states as $|0\rangle$ and $|1\rangle$, as shown in Fig. 1(a), except when it is clearly appropriate to adopt the Hund's case (a) and case (c) notation pertaining to bound and asymptotic configurations, respectively; likewise, the ground electronic state of the ion is designated as $|2\rangle$ at all interatomic separations.

[23] See, for example, Refs. [14,17].

[24] A. Fioretti, D. Comparat, C. Drag, T. F. Gallagher, and P. Pillet, Phys. Rev. Lett. **82**, 1839 (1999).

[25] C. Ospelkaus, S. Ospelkaus, L. Humbert, P. Ernst, K. Sengstock, and K. Bongs, Phys. Rev. Lett. **97**, 120402 (2006); M. Zaccanti, C. D'Errico, F. Ferlaino, G. Roati, M. Inguscio, and G. Modugno, Phys. Rev. A **74**, 041605(R) (2006).

[26] M. Dantus, R. M. Bowman, and A. H. Zewail, Nature (London) **343**, 737 (1990).

[27] J. A. Fleck, Jr., J. R. Morris, and M. D. Feit, Appl. Phys. **10**, 129 (1976); M. D. Feit, J. A. Fleck, Jr., and A. Steiger, J. Comput. Phys. **47**, 412 (1982).

[28] A. N. Hussain and G. Roberts, Phys. Rev. A **63**, 012703 (2000); **63**, 049902(E) (2001).